


RESEARCH

Open Access



Tumour-intrinsic PDL1 signals regulate the Chk2 DNA damage response in cancer cells and mediate resistance to Chk1 inhibitors

Clare E. Murray^{1†}, Anand V. R. Kornepati^{1,17†}, Carlos Ontiveros¹, Yiji Liao², Bárbara de la Peña Avalos³, Cody M. Rogers³, Zexuan Liu⁴, Yilun Deng⁴, Haiyan Bai², Suresh Kari⁴, Alvaro S. Padron⁴, Jacob T. Boyd¹, Ryan Reyes¹, Curtis A. Clark^{1,18}, Robert S. Svatek^{5,6}, Rong Li^{7,19}, Yanfen Hu^{7,20}, Meiling Wang³, José R. Conejo-García⁹, Lauren A. Byers¹⁰, Kavya Ramkumar¹⁰, Anil K. Sood¹¹, Jung-Min Lee¹², Christin E. Burd¹³ , Ratna K. Vadlamudi^{4,6}, Harshita B. Gupta³, Weixing Zhao³, Eloise Dray³, Patrick Sung^{3,6} and Tyler J. Curiel^{1,2,4,8,14,15,16,21*}

Abstract

Background Aside from the canonical role of PDL1 as a tumour surface-expressed immune checkpoint molecule, tumour-intrinsic PDL1 signals regulate non-canonical immunopathological pathways mediating treatment resistance whose significance, mechanisms, and therapeutic targeting remain incompletely understood. Recent reports implicate tumour-intrinsic PDL1 signals in the DNA damage response (DDR), including promoting homologous recombination DNA damage repair and mRNA stability of DDR proteins, but many mechanistic details remain undefined.

Methods We genetically depleted PDL1 from transplantable mouse and human cancer cell lines to understand consequences of tumour-intrinsic PDL1 signals in the DNA damage response. We complemented this work with studies of primary human tumours and inducible mouse tumours. We developed novel approaches to show tumour-intrinsic PDL1 signals in specific subcellular locations. We pharmacologically depleted tumour PDL1 in vivo in mouse models with repurposed FDA-approved drugs for proof-of-concept clinical translation studies.

Results We show that tumour-intrinsic PDL1 promotes the checkpoint kinase-2 (Chk2)-mediated DNA damage response. Intracellular but not surface-expressed PDL1 controlled Chk2 protein content post-translationally and independently of PD1 by antagonising PIRH2 E3 ligase-mediated Chk2 polyubiquitination and protein degradation. Genetic tumour PDL1 depletion specifically reduced tumour Chk2 content but not ATM, ATR, or Chk1 DDR proteins, enhanced Chk1 inhibitor (Chk1i) synthetic lethality in vitro in diverse human and murine tumour models, and improved Chk1i efficacy in vivo. Pharmacologic tumour PDL1 depletion with cefepime or ceftazidime replicated genetic tumour PDL1 depletion by reducing tumour Chk2, inducing Chk1i synthetic lethality in a tumour PDL1-dependent manner, and reducing in vivo tumour growth when combined with Chk1i.

[†]Clare E. Murray and Anand V. R. Kornepati contributed equally to this work.

*Correspondence:

tylerj.curiel@dartmouth.edu

tylerj.curiel@dartmouth.edu

Full list of author information is available at the end of the article



Conclusions Our data challenge the prevailing surface PDL1 paradigm, elucidate important and previously unappreciated roles for tumour-intrinsic PDL1 in regulating the ATM/Chk2 DNA damage response axis and E3 ligase-mediated protein degradation, suggest tumour PDL1 as a biomarker for Chk1i efficacy, and support the rapid clinical potential of pharmacologic tumour PDL1 depletion to treat selected cancers.

Keywords DNA damage repair, DDR inhibitors, Synthetic lethality, Immune checkpoints, PDL1, Chk2

Background

The immune co-signaling molecule programmed death ligand-1 (PDL1, *CD274*) is the target of successful FDA-approved cancer immunotherapies and is highly expressed in certain cancers [1, 2]. Surface-expressed tumour PDL1 increases immunopathogenicity by suppressing anti-tumour immune cells [3] through ligating their PD1 [4]. The principal mechanism-of-action of PDL1-blocking immunotherapy antibodies (α PDL1) is thought to be protecting PD1⁺ anti-tumour immune cells from inhibitory tumour surface-expressed PDL1 signals [2, 5, 6]. Although some individuals experience durable and/or complete treatment responses from α PDL1, most tumours (~85%) fail to respond [7, 8]. Thus, there is an incomplete mechanistic understanding of tumour PDL1 signaling and its relationship to tumour biology and treatment outcomes.

While surface-expressed tumour PDL1 effects on PD1⁺ anti-tumour T cells are well established, we and others identified non-canonical, tumour-intrinsic PDL1 signaling effects that are less understood but mediate various pro-tumour and treatment resistance programs that promote tumour pathogenesis [9]. Our group originally reported important tumour-intrinsic PDL1 signaling consequences, including promoting mTORC1 and tumour stemness and suppressing autophagy in melanoma and ovarian cancer cells [10, 11]. Targeting these or other tumour-intrinsic PDL1 signals through genetic and pharmacologic tumour PDL1 depletion improves various cancer treatments, including cytotoxic chemotherapy, autophagy inhibitors, mTORC1 inhibitors, and immune checkpoint blockade [12–15]. Nonetheless, clinically exploiting therapeutic vulnerabilities exposed from inhibiting tumour-intrinsic PDL1 is largely untapped and warrants further investigation.

Recently, we reported that genetic tumour PDL1 depletion impairs homologous recombination DNA damage repair [16]. Others reported that tumour PDL1 supports mRNA stability of DNA damage repair transcripts, but the relationship to DNA damage response (DDR) outcomes was not reported [17]. DDR is coordinated largely through the upstream ATM/Chk2 and ATR/Chk1 pathways that orchestrate DNA repair activation and cell cycle regulation [18]. Interference with the DDR offers opportunities for synthetic lethal approaches using small molecule DDR inhibitors (DDRi), some of which are in

clinical trials as single agents or in combination with α PDL1 or α PD1 immunotherapy [19]. However, there is an incomplete understanding of DDR mechanisms, DDRi treatment response biomarkers, and DDRi resistance mechanisms, warranting further investigation to understand tumour DDR biology and inform improved DDRi combination treatment regimens.

Whether tumour-intrinsic PDL1 modulates ATM/Chk2 or ATR/Chk1-mediated DDR is unreported. As we reported that tumour PDL1 supports BRCA1-mediated homologous recombination DNA damage repair pathway [16] that is downstream of ATM/Chk2 and ATR/Chk1 signals [20, 21], we hypothesised that tumour PDL1 could enhance the DDR through these DNA damage-induced signaling cascades. Here we present functional, biochemical, and molecular evidence that tumour-intrinsic PDL1 specifically promotes Chk2 protein stability by suppressing Chk2 polyubiquitination. Genetically silencing tumour PDL1 in multiple tumour models, including cell lines derived from our novel autochthonous melanoma model, reduced Chk2 signals without impairing the ATR/Chk1 axis and improved sensitivity to selective small molecule Chk1 inhibitors (Chk1i) and ATR inhibitors (ATRi) both in vitro and in vivo, demonstrating a synthetic lethal interaction between tumour PDL1 depletion and ATR/Chk1 inhibition. Intracellular but not surface PDL1 promotes Chk2 protein content and Chk1i treatment resistance, whereas surface PDL1 mediated distinct tumour-intrinsic signaling outcomes. We recently discovered that the β -lactam antibiotics cefepime and ceftazidime deplete tumour PDL1 [15]. Here we report that these agents phenocopy genetic PDL1 depletion effects to deplete tumour Chk2 protein, induce DNA damage, and enhance PDL1-dependent Chk1i synthetic lethality, demonstrating a clinical translation potential of these novel tumour-intrinsic PDL1 mechanistic controls.

Results

Tumour PDL1 promotes Chk2-mediated DNA damage responses

To study the role of PDL1 in the ATM/Chk2 and ATR/Chk1 DDR axes, we initially utilized B16 mouse melanoma and ES2 human ovarian cancer cells which basally express high levels of PDL1 and generated genetic PDL1

knockouts (PDL1^{KO}) by CRISPR/Cas9. We have previously defined significant tumour PDL1-controlled pathologic pathways in these models [10, 11]. RNA-sequencing and gene set enrichment analysis of PDL1^{KO} versus CTRL B16 mouse melanoma cells identified multiple pathways influenced by tumour PDL1 silencing (Fig. S1a), consistent with our prior reports [10, 11]. Interestingly, pathways associated with DDR checkpoints were among those most significantly altered by PDL1 loss (Fig. S1a), including downregulation of the p53 pathway in PDL1^{KO} versus CTRL. Significant genes driving enrichment of each hallmark pathway are detailed in Table S1. Upregulated pathways in PDL1^{KO}, including mitotic spindle, G2/M checkpoint, and E2F targets, could suggest increased cell proliferation. However, PDL1 depletion from tumour cells generally reduces *in vitro* cell proliferation as we and others have reported [9, 10, 22]. We tested additional unreported human and mouse PDL1-depleted cell lines and found that genetic PDL1 also slowed their growth

in vitro (Fig. S1b). Interrogation of DDR signaling axes ATM/Chk2 and ATR/Chk1 by immunoblotting identified specific total Chk2 protein reduction in cultured, otherwise unperturbed PDL1^{KO} B16 mouse melanoma cells and PDL1^{KO} ES2 human ovarian cancer cells without significantly altered ATM, ATR, or Chk1 DDR proteins compared to respective CTRL cells (Fig. 1a,b). Chk2 nuclear foci were significantly decreased in PDL1^{KO} B16 cells by immunofluorescence (Fig. S1c), consistent with immunoblot data (Fig. 1a,b). γ H2AX, a surrogate marker for DNA double strand breaks [23, 24], accumulated even under homeostatic conditions in PDL1^{KO} versus control B16 and ES2 cells (Fig. 1a,b), suggesting tumour PDL1 suppresses DNA damage accumulation in some tumour types experiencing high levels of endogenous cellular DNA damage stress. In further support, nuclear γ H2AX foci were significantly increased in PDL1^{KO} B16 cells by immunofluorescence (Fig. S1d). To determine PDL1 dependence of tumour Chk2 content, we transiently

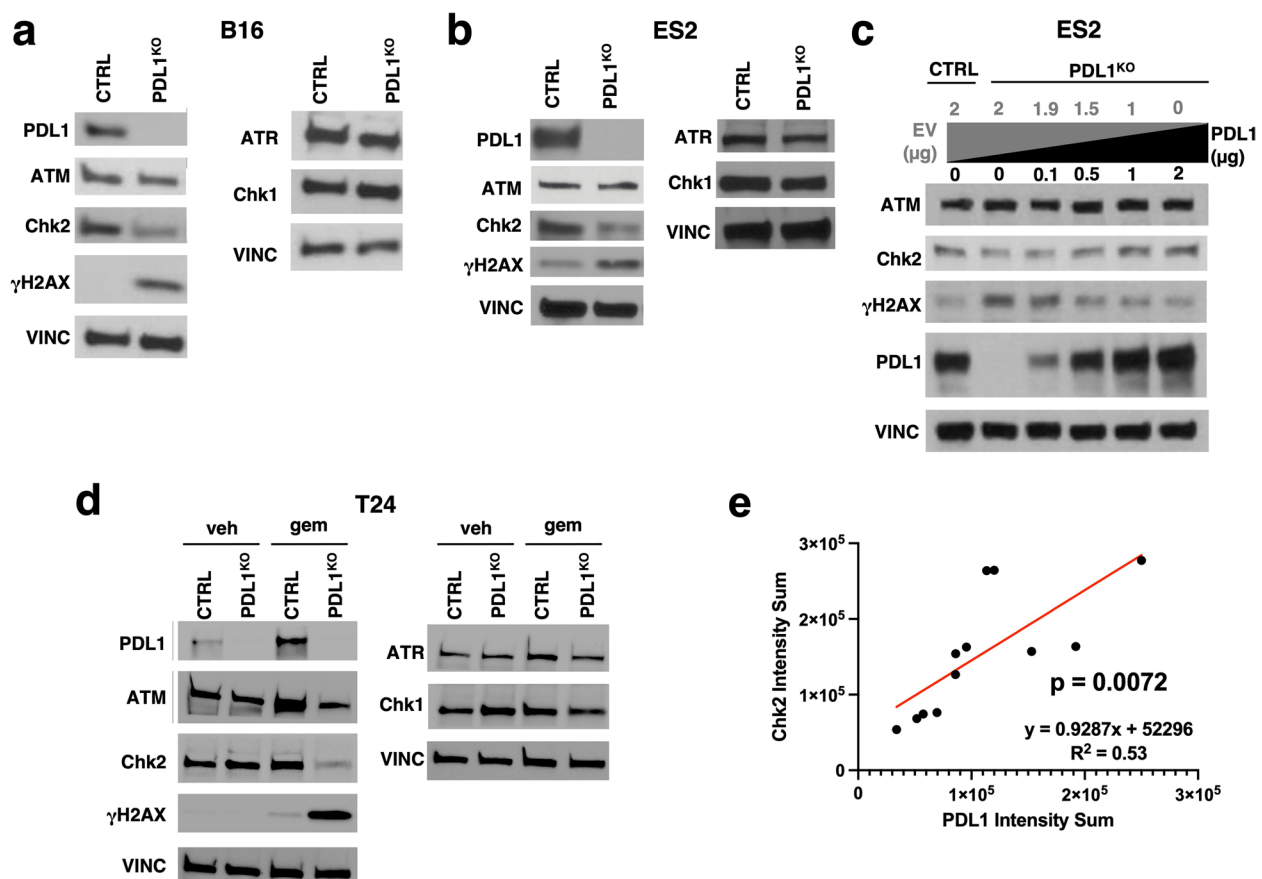


Fig. 1 Tumour PDL1 promotes Chk2 content. **a** Immunoblot from whole cell lysates of CTRL and PDL1^{KO} B16 cells. Vinculin (VINC), loading control. γ H2AX^{Ser139} blot is shown as γ H2AX. **b** Immunoblot from whole cell lysates of CTRL and PDL1^{KO} ES2 cells. VINC, loading control. **c** Immunoblot of CTRL and PDL1^{KO} ES2 cells transfected with empty vector (EV, gray) and/or PDL1 plasmid (black) at depicted μ g. **d** Immunoblot of CTRL versus PDL1^{KO} T24 cells after 72-h incubation with vehicle or gemcitabine (5 ng/mL). **e** Quantification of relative intracellular PDL1 and Chk2 expression of 12 human high-grade serous ovarian tumours at upfront treatment. Statistical analysis by linear regression

re-expressed PDL1 at increasing concentrations in PDL1^{KO} ES2 cells and observed a direct increase in Chk2 and simultaneous decrease in γ H2AX as PDL1 content increased, further showing that Chk2 protein reduction from PDL1 depletion resulted in significant increases in DNA damage (Fig. 1c). We also flow sorted cultured, otherwise unperturbed CTRL ES2 cells into the highest (PDL1^{hi}) and lowest (PDL1^{lo}) PDL1 expressing cells and found that PDL1^{lo} cells have significantly less Chk2 protein, which further supports PDL1 promotion of Chk2 content to suppress DNA damage (Fig. S1e).

As some cell lines exhibit relatively lower basal PDL1 content compared to B16 or ES2 cells, which could be from lower endogenous DNA damage stress, we investigated the possibility that Chk2-mediated DDR signaling could be further impaired from exogenous sources of DNA damage in specific PDL1-deficient cells. We used PDL1^{KO} T24 human bladder cancer cells that exhibit many known tumour-intrinsic PDL1 depletion outcomes [25] and observed decreased Chk2 in them only after exogenous DNA damage induction with cytotoxic gemcitabine, while the ATR/Chk1 pathway remained unaffected (Fig. 1d). PDL1^{KO} T24 cells also accumulated more γ H2AX versus CTRL T24 cells with gemcitabine by immunoblot, corroborated by confocal imaging of γ H2AX nuclear foci (Fig. S1f), consistent with a report in breast and colon cancer cells [17]. In addition, function-related phospho-Chk2 was significantly decreased specifically in PDL1^{KO} T24 cells with gemcitabine treatment, supporting decreased Chk2 activity (Fig. S1g). Thus, basal DNA damage from homeostatic processes is sufficient to reduce Chk2 protein in some PDL1^{KO} cells (e.g., B16, ES2), whereas induction of additional DNA damage is required to reduce Chk2 content in other PDL1^{KO} cell lines (e.g., T24). To confirm human relevance, we analysed 12 high-grade serous ovarian cancer patient samples from patients receiving first-line treatment and identified a significant positive correlation between tumour PDL1 and Chk2 (Fig. 1e, Fig. S1h), confirming tumour PDL1 can predict Chk2 in primary human tumours.

Genetic tumour PDL1 depletion enhances tumour Chk1i synthetic lethality

As ATM/Chk2 and ATR/Chk1 axes are distinct yet coordinated and compensatory pathways that initiate effective DNA repair [26, 27], we hypothesised that inhibiting the ATR/Chk1 axis could induce synthetic lethality in PDL1-deficient tumour cells based on compromised Chk2-mediated DDR. We generated several additional PDL1-deficient cell lines (Fig. S2a-c), all of which were significantly more sensitive to the Chk1i rabusertib versus respective CTRL cells in vitro (Fig. 2a). PDL1^{KO} B16

cells were also significantly more sensitive to the more potent Chk1i prexasertib versus CTRL cells in vitro (Fig. S2d). PDL1-depleted T24 and 4T1 cells were more easily killed by Chk1i as assessed by Annexin V/PI staining (Fig. 2b-c) and validated by colony formation assays (Fig. 2d), confirming *bona fide* synthetic lethality, further supported by reduced viable cell counts of PDL1^{lo} versus CTRL 4T1 cells after rabusertib (Fig. S2e). Gemcitabine also substantially reduced PDL1^{KO} T24 cell numbers (Fig. S2f), supporting impaired DDR in PDL1^{KO} T24 cells that creates sensitivity to DNA-damaging agents. PDL1-deficient cells were also significantly more sensitive to the selective ATRi AZD6738 (Fig. 2e), although less so than with Chk1i, but PDL1^{KO} T24 cells were not significantly sensitive to ATMi AZD0156 (Fig. 2f), all supporting specific Chk2 deficiency in PDL1-depleted tumour cells. Differential ATRi sensitivity could relate to increased p-Chk1 in some cases of tumour PDL1 depletion (e.g., Fig. S1g), which itself could be compensatory to reduced p-Chk2. Chk2 inhibition with the validated small molecule Chk2 inhibitor BML-277 improved both Chk1i and ATRi efficacy in 4T1 and ID8agg cells (Fig. S2g-j), though Chk1i sensitivity was superior versus ATRi, mirroring our PDL1 depletion data and supporting that Chk2 inhibition improves sensitivity to both Chk1i and ATRi in cell lines used here.

Using a published dataset [28], we segregated 44 recently-derived primary ASCL1 subtype (SCLC-A) human small cell lung cancer lines into PDL1^{lo} or PDL1^{hi} cells by median centered analysis. Strikingly, we found that PDL1^{lo} SCLC-A cells were significantly (1.87-fold) more sensitive to Chk1i versus PDL1^{hi} cells in vitro and ATMi-resistant as expected (Fig. 2g-h). As some variant data points could have outsized effects on this limited data set, we performed Grubb's test, which did not detect outlier data points. PDL1^{lo} SCLC-A cells trended to greater ATRi-sensitivity versus PDL1^{hi} cells (Fig. S2k) without reaching statistical significance. We further validated that total Chk2 protein is depleted in PDL1^{lo} versus CTRL MDA-MB-231 after rabusertib incubation by immunoblot while ATR and Chk1 content were unaffected (Fig. S2l).

Tumour PDL1-dependent Chk1i synthetic lethality resistance is Chk2-dependent

We re-expressed Chk2 (Chk2^{RE}) in PDL1-depleted cells, which fully restored Chk2 protein in PDL1^{lo} 4T1 cells and reversed DNA damage accumulation following Chk1i treatment (Fig. 2i) with similar data in CTRL versus PDL1^{KO} Chk2^{RE} T24 cells (Fig. S2m). Consistent with these data, Chk2^{RE} fully reversed Chk1i synthetic lethality in PDL1^{lo} 4T1 cells (Fig. 2j) and PDL1^{lo} MDA-MB-231 cells (Fig. S2n-o). By contrast, synthetic lethality

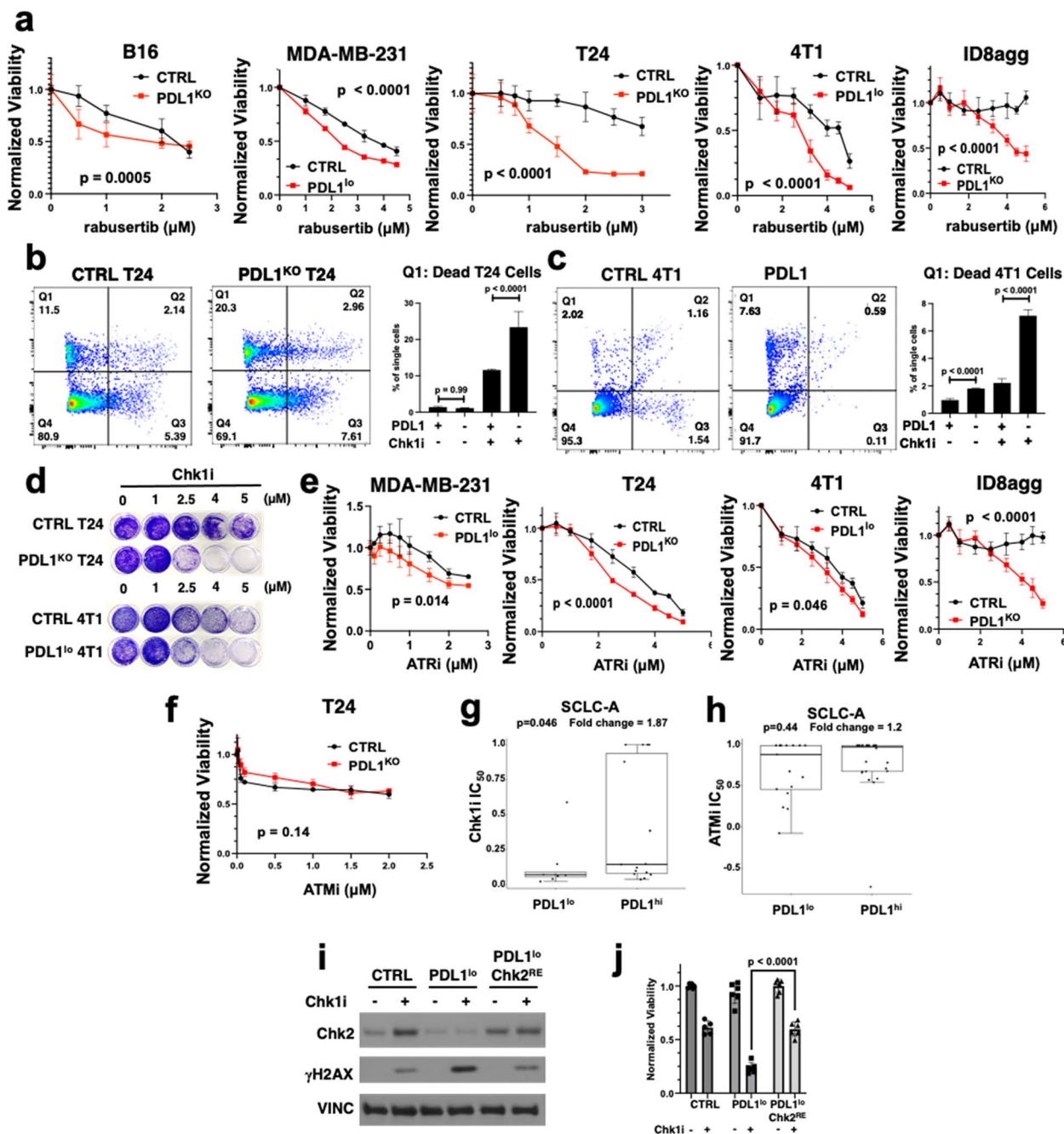


Fig. 2 Tumour PDL1 deficiency promotes Chk2-dependent synthetic lethality to Chk1i and ATRi in vitro. **a**. In vitro cell viability of CTRL versus PDL1^{KO} B16, T24, and ID8agg cells or CTRL versus PDL1^{lo} 4T1 and MDA-MB-231 cells incubated with the selective Chk1i rabusertib for 5 days at indicated doses (mean \pm SD, $n = 3$ independent replicates, P values by two-way ANOVA). Viability normalised to vehicle controls. **b**. Flow cytometry analysis of Annexin/PI-stained CTRL versus PDL1^{KO} T24 cells and **c**. CTRL versus PDL1^{lo} 4T1 cells after treatment with vehicle (DMSO) or 1 μ M rabusertib. Q1 (% dead cells) quantified. P , two-way ANOVA. **d**. Clonogenic crystal violet stain of PDL1^{KO} T24 or PDL1^{lo} 4T1 and respective CTRL cells treated with indicated rabusertib (Chk1i) concentrations for 5 days. **e**. Cell viability of indicated CTRL versus PDL1-deficient cell lines after ATRi (AZD6738) or **f**. ATMi (AZD0156) incubation. P , two-way ANOVA. **g**. IC₅₀ for the Chk1i prexasertib and **h**. ATMi AZD0156 in 44 human SCLC-A cell lines segregated by low (lo) or high (hi) PDL1 expression. P , two-sided t -test. Grubb's test was used to identify outliers. **i**. Immunoblot after Chk2 re-expression plasmids (Chk2^{RE}) or empty vector controls were transiently introduced into CTRL or PDL1^{lo} 4T1 cells and treated with rabusertib (Chk1i, 2.5 μ M) or vehicle (DMSO) for 72 h. **j**. PDL1^{lo} 4T1 viability with transient Chk2^{RE} as in **i**, treated with 2.5 μ M rabusertib for 5 days in vitro versus CTRL and PDL1^{lo} with empty vector. Data are mean \pm SD normalised to vehicle. P , unpaired t -test

resistance to Chk1i was only partially restored by Chk2^{RE} in PDL1^{KO} T24 cells (Fig. S2p). Thus, in selected tumours, PDL1-mediated synthetic lethality resistance to Chk1i could include additional factors aside from Chk2. Based on potential p53 effects discerned in RNA-seq data, we incubated T24 cells with rabusertib ± the small molecule p53 activator nutlin-3a or p53 inhibitor pifithrin- α to find they did not alter PDL1-dependent synthetic lethality to rabusertib (Fig. S2q-r).

Genetic tumour PDL1 depletion promotes Chk1i synthetic lethality in vivo

We challenged severely immunodeficient female NOD.SCID γ c-deficient (NSG) mice with CTRL or PDL1^{lo} 4T1 cells in mammary fat pads and treated with the Chk1i rabusertib. PDL1^{lo} but not CTRL 4T1 tumours in NSG females were exquisitely sensitive to single agent rabusertib (Fig. 3a-c), supporting immune-independent Chk1i sensitivity in PDL1^{lo} 4T1 tumours. However, PDL1^{KO} B16 tumours did not respond to rabusertib in NSG mice (Fig. 3d-f), suggesting an immune requirement for Chk1i efficacy in vivo. CTRL B16 tumours implanted into immune-competent wild type (WT) C57/Bl6 mice were refractory to rabusertib treatment in vivo whereas PDL1^{KO} B16 tumours were highly rabusertib-sensitive (Fig. 3g-i). Flow cytometry of tumour-infiltrating immune cells showed that rabusertib significantly increased total and granzyme B⁺ (GzB) CD8⁺ T cells and GzB mean fluorescence intensity (MFI, per-cell production) in the tumour microenvironment (Fig. 3j-l), increased interferon (IFN) γ ⁺ CD8⁺ T cells and IFN γ MFI (Fig. S3a-b), and increased natural killer cell GzB MFI (Fig. S3c-d) in PDL1^{KO} but not CTRL B16 tumours. These immune cell populations mediate anti-tumour immunity¹, supporting improved anti-tumour immunity in PDL1^{KO} tumours treated with Chk1i. Prevalence of other prominent tumour microenvironmental immune cells, including regulatory T cells, myeloid cells, dendritic cells, macrophages, and myeloid derived suppressor cells, were unchanged with Chk1i treatment in PDL1^{KO} versus CTRL tumours, (Fig. S3e-p), except decreased CD4⁺ T cells and B cells in rabusertib-treated PDL1^{KO} B16

tumours versus vehicle-treated tumours (Fig. S3q-r). To support adaptive immune contributions to Chk1i efficacy in PDL1^{KO} B16 tumours, we challenged Rag2^{KO} mice with PDL1^{KO} B16 cells and found abolished rabusertib efficacy (Fig. 3m-n). Collectively, these data support tumour-intrinsic PDL1 control of Chk2 DDR improves Chk1i efficacy in vivo by an immune-independent or immune-dependent mechanism in distinct tumours, and that tumour PDL1 control of Chk2 alters anti-tumour immunity independent of its known tumour-extrinsic signaling effects on PD1⁺ immune cells that is not specific to breast cancer, melanoma, genetic background, or tumour microenvironment.

Autochthonous PDL1-deficient tumour cells phenocopy genetic PDL1 silencing in Chk2 deficiency and Chk1i synthetic lethality

To date, essentially all reports describing tumour-intrinsic PDL1 signaling consequences use genetic PDL1 depletion in established PDL1-expressing tumour cells. We generated a novel murine autochthonous melanoma model wherein mice lack PDL1 only in melanocytes, the melanoma cell-of-origin, and develop *Nras*^{Q61R} melanomas de novo by 4-hydroxytamoxifen induction (see Methods). We crossed a mouse with *CD274* flanked by LoxP sites with a Tyrosinase:Cre^{ERT2} inducible *Nras*^{Q61R} (*TN*^{61R}) mouse²⁹. Melanocyte PDL1-deficient mice (*CD274*^{fl/fl} *TN*^{61R}) and PDL1-replete littermate controls (*CD274*^{+/+} *TN*^{61R}) develop PDL1-null (PDL1⁻) or PDL1-replete (PDL1⁺) melanomas, respectively from the time of initiation. We cultured single cell suspensions from autochthonous tumours from these mice in vitro and generated PDL1⁺ NCH1 and PDL1⁻ NFH1 *Nras*^{Q61R} melanoma cell lines. We confirmed lack of basal and IFN γ -inducible PDL1 expression in PDL1⁻ NFH1 versus PDL1⁺ NCH1 cells (Fig. 4a). PDL1⁻ NFH1 cells exhibited decreased Chk2 protein content and increased γ H2AX after rabusertib treatment versus PDL1⁺ NCH1 cells (Fig. 4b). PDL1⁻ NFH1 cells exhibited increased sensitivity to Chk1i rabusertib and prexasertib in vitro versus PDL1⁺ NCH1 cells (Fig. 4c-d), consistent with data from genetically depleting PDL1 from established

(See figure on next page.)

Fig. 3 Tumour PDL1 depletion promotes Chk1i synthetic lethality in vivo that requires adaptive immunity in distinct models. Growth in mammary fat pad of **a**. CTRL and **b**. PDL1^{lo} 4T1 tumours in immune deficient NSG mice treated with vehicle or rabusertib (Chk1i). Data represented as mean \pm SEM. *P* by two-way ANOVA. **c**. Tumour end-point weights from **a** and **b**. *P*, unpaired *t*-test. **d-e**. Tumour growth curves of NSG mice challenged with **d**. CTRL and **e**. PDL1^{KO} B16 cells and treated with rabusertib daily. *P*, two-way ANOVA. **f**. NSG mice bearing B16 tumours as in **d-e** were sacrificed day 21 post-challenge and tumours were weighed. *P*, unpaired *t*-test. **g-h**. Growth of subcutaneous **g**. CTRL versus **h**. PDL1^{KO} B16 tumours in WT mice treated with vehicle or rabusertib. Data represented as mean \pm SEM. *P*, two-way ANOVA. **i**. Tumour end-point weights from **g** and **h**. *P*, unpaired *t*-test. **j-l**. Flow cytometry immune analyses of indicated populations in CTRL versus PDL1^{KO} B16 tumours treated with vehicle or rabusertib in vivo. Mice were sacrificed day 17 post-challenge. *P*, unpaired *t*-test. **m**. Tumour growth curves of Rag2^{KO} mice bearing PDL1^{KO} B16 tumours treated with vehicle or rabusertib daily. *P*, two-way ANOVA. **n**. Rag2^{KO} mice as in **m** were sacrificed day 20 post-challenge. *P*, unpaired *t*-test

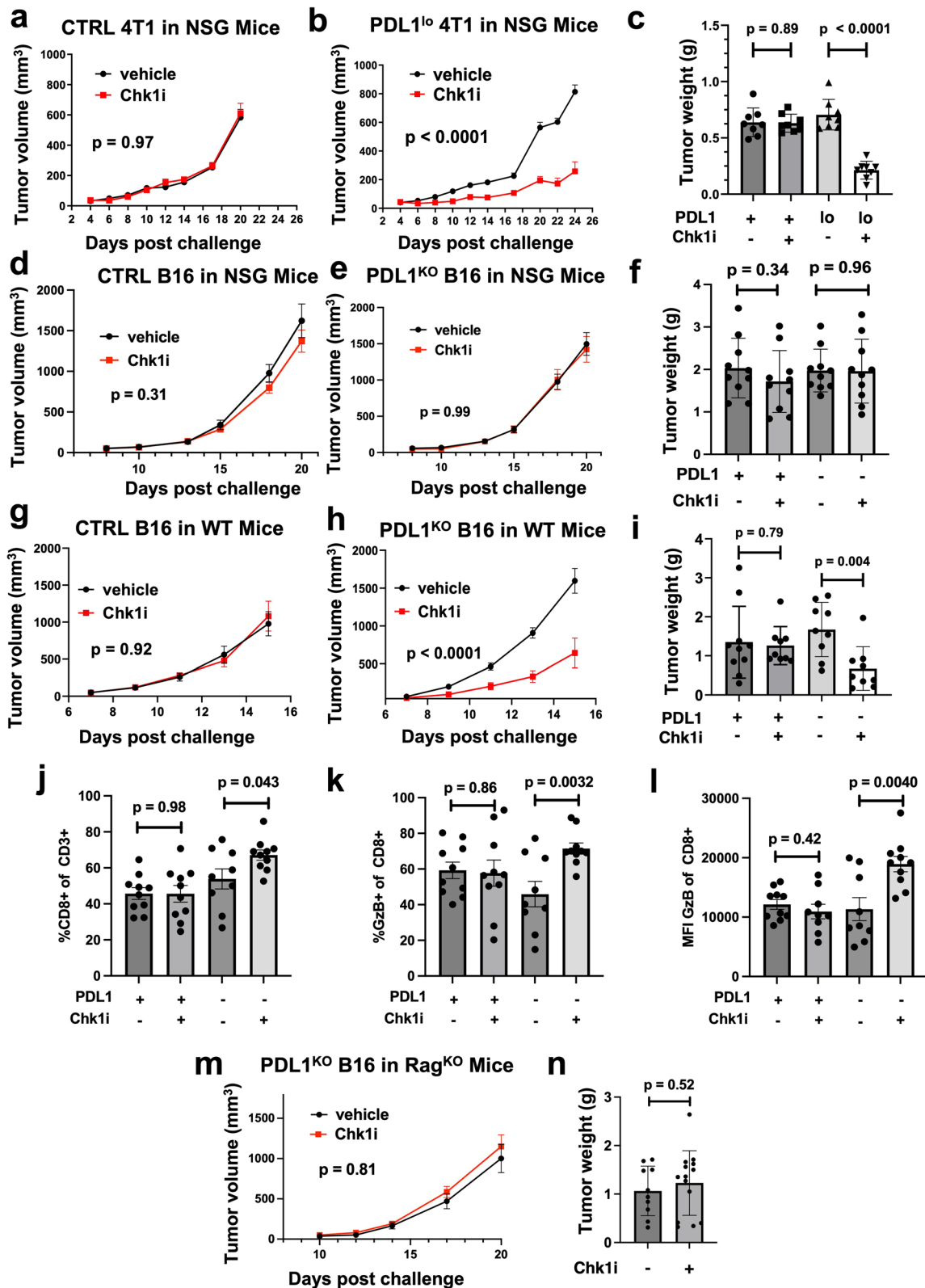


Fig. 3 (See legend on previous page.)

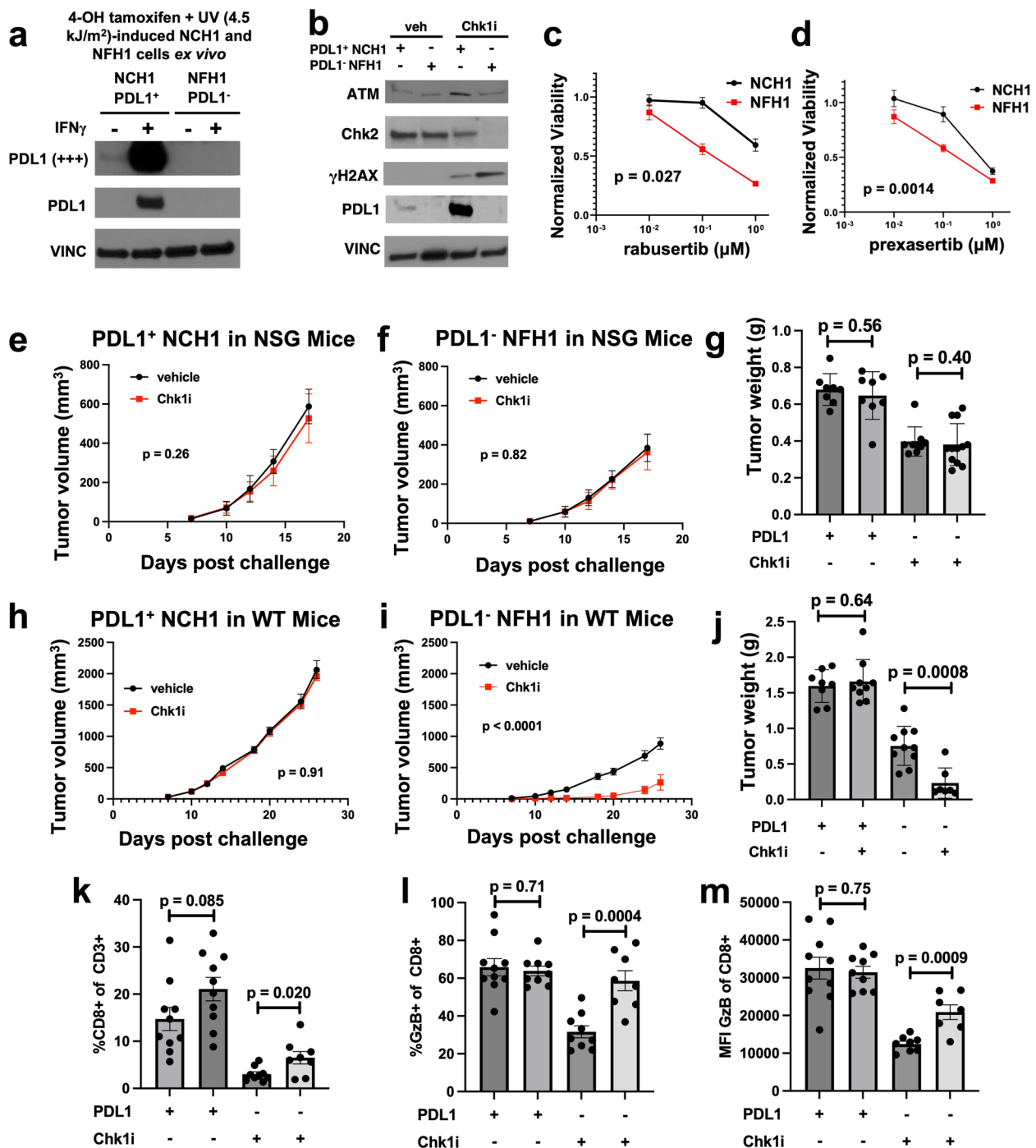


Fig. 4 Autochthonous PDL1-deficient tumour cells phenocopy genetic PDL1 silencing by inducing Chk2 deficiency and Chk1i synthetic lethality in vitro and in vivo. **a** Immunoblot validation of PDL1 expression in *NRAS*^{G61R}-mutant melanoma cells derived from CTRL *TN*^{G1R} (NCH1; PDL1⁺) or PDL1⁻ *TN*^{G1R} (NFH1; PDL1⁻) mice. Cells were treated in vitro with 0.1 ng/mL IFN γ for 48 h. **b** Immunoblot of NCH1 (PDL1⁺) or NFH1 (PDL1⁻) cells treated in vitro with the Chk1i rabusertib or vehicle (veh) for indicated proteins. **c-d**. Cell viability of PDL1⁺ NCH1 versus PDL1⁻ NFH1 melanoma cells treated with the Chk1i c. rabusertib or d. prexasertib for 72 h in vitro. Viability normalised to vehicle. *P*, two-way ANOVA. NSG mice were challenged with e. PDL1⁺ NCH1 cells or f. PDL1⁻ NFH1 cells and treated with rabusertib daily. *P*, two-way ANOVA. **g**. Tumour-bearing NSG mice were sacrificed day 18 post-challenge. Tumours were excised and weighed. *P*, unpaired *t*-test. WT mice were challenged with h. NCH1 or i. NFH1 cells and treated with vehicle or rabusertib daily. *P*, two-way ANOVA. **j**. Tumour-bearing WT mice were sacrificed, and tumours were excised and weighed. *P*, unpaired *t*-test. **k-m**. WT mice bearing NCH1 or NFH1 tumours were sacrificed day 28 post-challenge and profiled for indicated immune populations by flow cytometry. MFI, mean fluorescence intensity. *P*, unpaired *t*-test

tumour cells. However, similarly to the B16 melanoma model, PDL1⁻ NFH1 tumours did not respond to rabusertib in vivo when challenged into immunodeficient NSG mice (Fig. 4e-g). In syngeneic WT mice, rabusertib significantly suppressed in vivo growth of PDL1⁻ NFH1 versus PDL1⁺ NCH1 tumours (Fig. 4h-j). Immune profiling of NCH1 and NFH1 tumours revealed rabusertib significantly increased total and GzB⁺ CD8⁺ T cells and their GzB production by MFI (Fig. 4k-m) in PDL1⁻ NFH1 tumours, similar to rabusertib-treated PDL1^{KO} B16 tumours. Other immune populations assessed as in Fig. S3 were not significantly changed (Fig. S4a-r). Thus, PDL1 effects on the Chk2-mediated DNA damage response and Chk1i sensitivity are not from compensatory mechanisms following PDL1 depletion from established PDL1-expressing tumours, as NFH1 tumours never expressed PDL1.

Non-surface tumour PDL1 supports Chk2 protein content and blunts Chk1i synthetic lethality

Tumour-expressed PD1 can drive tumour surface PDL1-dependent signals, such as promoting cell proliferation, mTORC1 activation, and inducing tumour surface PDL1 reverse signaling, including in B16 cells studied here [9]. Immunoblots demonstrated that γ H2AX, ATM/Chk2, and ATR/Chk1 were unaffected by PD1^{KO} in B16 cells (Fig. 5a), supporting PD1-independent tumour PDL1 control of Chk2. In support, neither genetic PD1 depletion of T24 cells (validated in Fig. S5a) nor surface PD1-blocking antibodies enhanced their Chk1i synthetic lethality (Fig. 5b). Thus, tumour PDL1 control of Chk2 and Chk1i sensitivity is PD1-independent in distinct mouse and human cancer cells.

Membrane-bound PDL1 can signal extrinsically from the tumour surface and contains a 30 amino acid cytoplasmic C-terminal tail unlikely to mediate significant tumour-intrinsic signaling from the surface [30], but PDL1 is also distributed throughout the cytoplasm and nucleus [31–34]. We re-expressed PDL1 in PDL1^{KO} B16 cells in a vector generating preferential membrane expression (PDL1^{mem}) or a vector expressing preferential cytoplasmic PDL1 (PDL1^{cyto}) (Fig. 5c, Fig. S5b-c, see Methods) to understand the impact of subcellular PDL1 distribution on tumour-intrinsic signaling consequences. PDL1^{mem} mediated a gene-expression profile clearly distinct from PDL1^{cyto} (Fig. 5d), consistent with distinct functional outcomes of subcellular PDL1 expression. A GSEA signature associated with G2/M checkpoints and E2F targets was more enriched in PDL1^{cyto}, while a GSEA signature associated with an epithelial to mesenchymal transition signature was significantly enriched in PDL1^{mem} cells (Fig. 5d). As Chk2 also activates p53 and E2F signaling and regulates mitotic spindle assembly [35,

36], we considered that surface PDL1 was unlikely to regulate Chk2 protein expression but that fully intracellular (non-surface membrane) PDL1 could. In support, PDL1^{mem} did not restore Chk2 protein content or reduce γ H2AX accumulation by immunoblot, whereas PDL1^{cyto} rescued both phenotypes (Fig. 5e, quantified in Fig. S5d). By contrast, PDL1^{mem} enhanced vimentin expression, an epithelial to mesenchymal transition marker [37], distinct from PDL1^{cyto} (Fig. 5e, Fig. S5d) and consistent with our RNA-seq data. To confirm the non-surface PDL1 role in Chk1i synthetic lethality, we showed that PDL1^{mem} versus PDL1^{cyto} cells were more significantly killed by the Chk1 inhibitors rabusertib (Fig. 5f) and prexasertib (Fig. S5e). Our findings are consistent with previous studies that showed specific functions of subcellular PDL1 [17, 33, 34]. Thus, tumour PDL1 in specific subcellular locations affects distinct signals and functions, including control of Chk2 protein content distinctly by cytoplasmic PDL1.

Interferon- γ and tumour necrosis factor- α preferentially increase tumour membrane PDL1 without affecting Chk1i synthetic lethality

Interferon- γ (IFN γ) and tumour necrosis factor- α (TNF α) are anti-tumour cytokines that increase tumour surface PDL1 expression, but their effects on subcellular PDL1 are little reported except to show that they minimally induce nuclear PDL1 [34]. As their PDL1 control mechanisms differ, and tumour PDL1 induced by IFN γ versus TNF α alters tumour biology distinctly [38], we considered that they could also differentially affect tumour-intrinsic PDL1 signals. We confirmed that each cytokine robustly induced total PDL1 content in T24 and 4T1 cell lines as expected (Fig. S6a-b). However, neither IFN γ nor TNF α -induced PDL1 appreciably altered rabusertib synthetic lethality in T24 or 4T1 cells (Fig. 5g, Fig. S6c), suggesting lack of preferential cytoplasmic PDL1 induction. We then assessed subcellular PDL1 to find that each cytokine preferentially induced surface membrane but not cytoplasmic PDL1 in T24 cells and 4T1 cells (Fig. 5h, Fig. S6d), consistent with our data that cytoplasmic tumour PDL1 promotes Chk2 content as a distinct function from membrane-bound PDL1.

PDL1 inhibits Chk2 ubiquitination and degradation

Tumour-intrinsic PDL1 in specific subcellular locations can increase cytoplasmic mRNA stability [17] or act as a nuclear co-transcription factor [33, 34]. However, transcripts of several DDR proteins, including *Chk2*, were not significantly different between CTRL and PDL1^{KO} B16 cells in our RNA-seq datasets (Fig. 6a). In support, *Chk2* mRNA levels were unchanged at baseline and following rabusertib treatment in CTRL and PDL1^{KO} B16

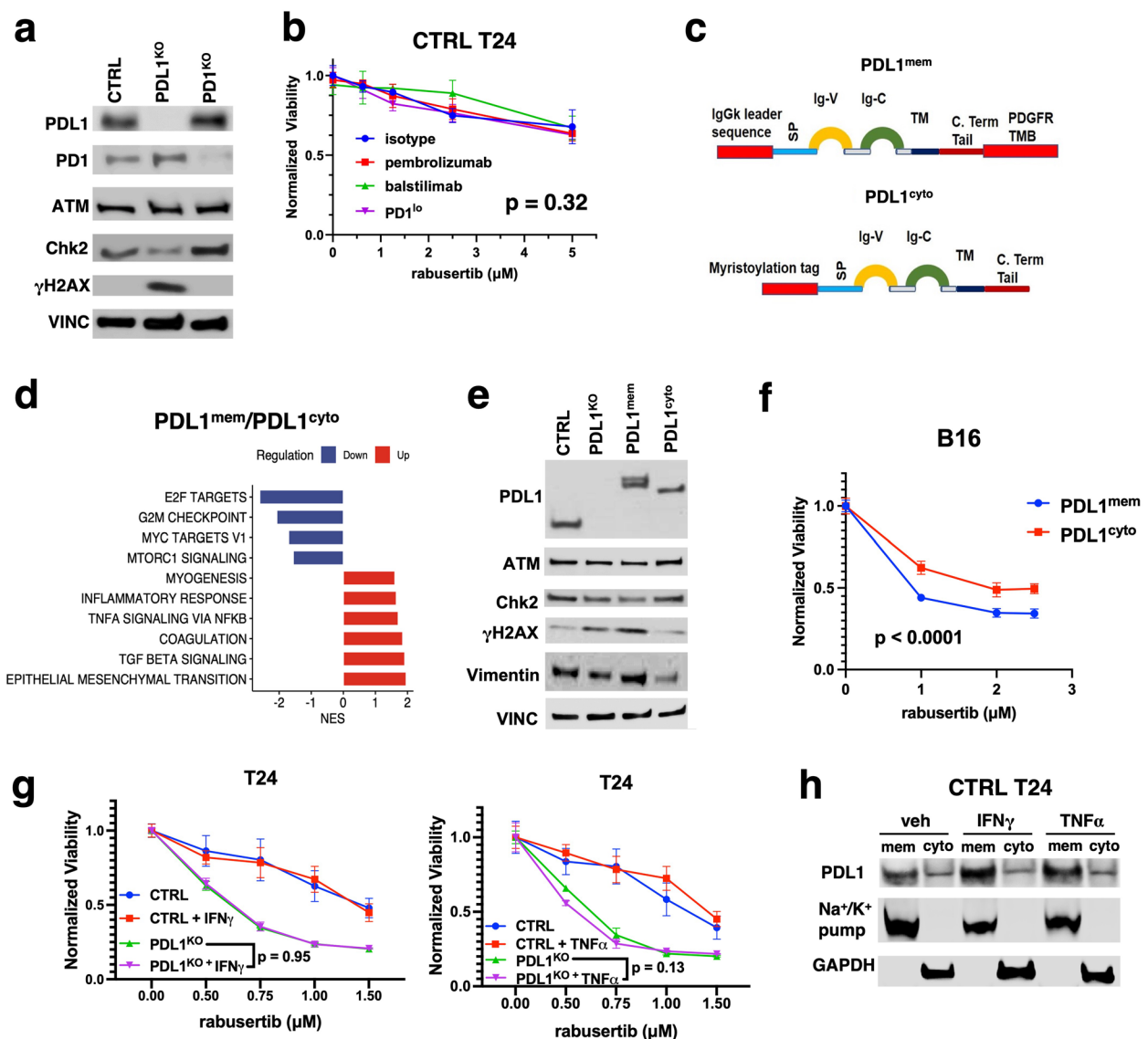


Fig. 5 Tumour PDL1 control of Chk2 is through intracellular PDL1 and independent of PD1 and immunity. **a**. Immunoblots of PDL1^{KO} and PD1^{KO} B16 cells versus CTRL B16 cells for indicated proteins. Vinculin (VINC) loading control. **b**. In vitro MTT cell viability of CTRL T24 cells treated with the αPD1 antibodies pembrolizumab (50 μg/mL), balstilimab (50 μg/mL), or genetic shRNA PD1 knockdown (PD1^{lo}) with increasing doses of the Chk1i rabusertib for 5 days at indicated doses. *P* by two-way ANOVA. Viability shown as relative values following normalisation to respective isotype or vehicle-treated controls. **c**. Schematic of membrane (mem)-localising versus intracellular (cyto)-localising PDL1 expression constructs (see methods). **d**. RNA-seq analyses of PDL1^{mem} versus PDL1^{cyto} B16 cells using gene set enrichment analysis. Top 10 altered hallmark pathways (*p* < 0.01) are shown by PDL1 subcellular location. **e**. Immunoblot comparing ATM, Chk2, γH2AX, and vimentin expression of indicated B16 cells. Vinculin (VINC) as loading control. **f**. MTT viability assay of PDL1^{mem} versus PDL1^{cyto} cells after 96-h of in vitro treatment with the Chk1i rabusertib at indicated concentrations. *P*, two-way ANOVA. **g**. Viability analysis of CTRL versus PDL1^{KO} T24 cells treated with indicated rabusertib concentrations ± 1 ng/mL IFN_γ, 10 ng/mL TNFα, or vehicle. *P*, two-way ANOVA. **h**. Immunoblot of cell lysates of membrane and cytosolic fractions of CTRL T24 cells treated with vehicle (PBS), IFN_γ, or TNFα as in **g**. Na⁺/K⁺ pump as membrane loading control and GAPDH as cytosolic loading control.

cells (Fig. 6b) despite decreased baseline Chk2 protein, suggesting PDL1 regulation of Chk2 independent of transcriptional regulation or mRNA stability. We reported that tumour-intrinsic PDL1 promotes mTORC1 activation in B16 cells [10] that can enhance mRNA translation. However, genetic knockdown of Raptor, the principal

component of the mTORC1 complex, did not affect Chk2 protein content in B16 cells (Fig. S7). Chk2 protein half-life but not ATM protein half-life was greatly reduced in PDL1^{KO} versus CTRL B16 cells (Fig. 6c), consistent with PDL1 post-translational Chk2 control.

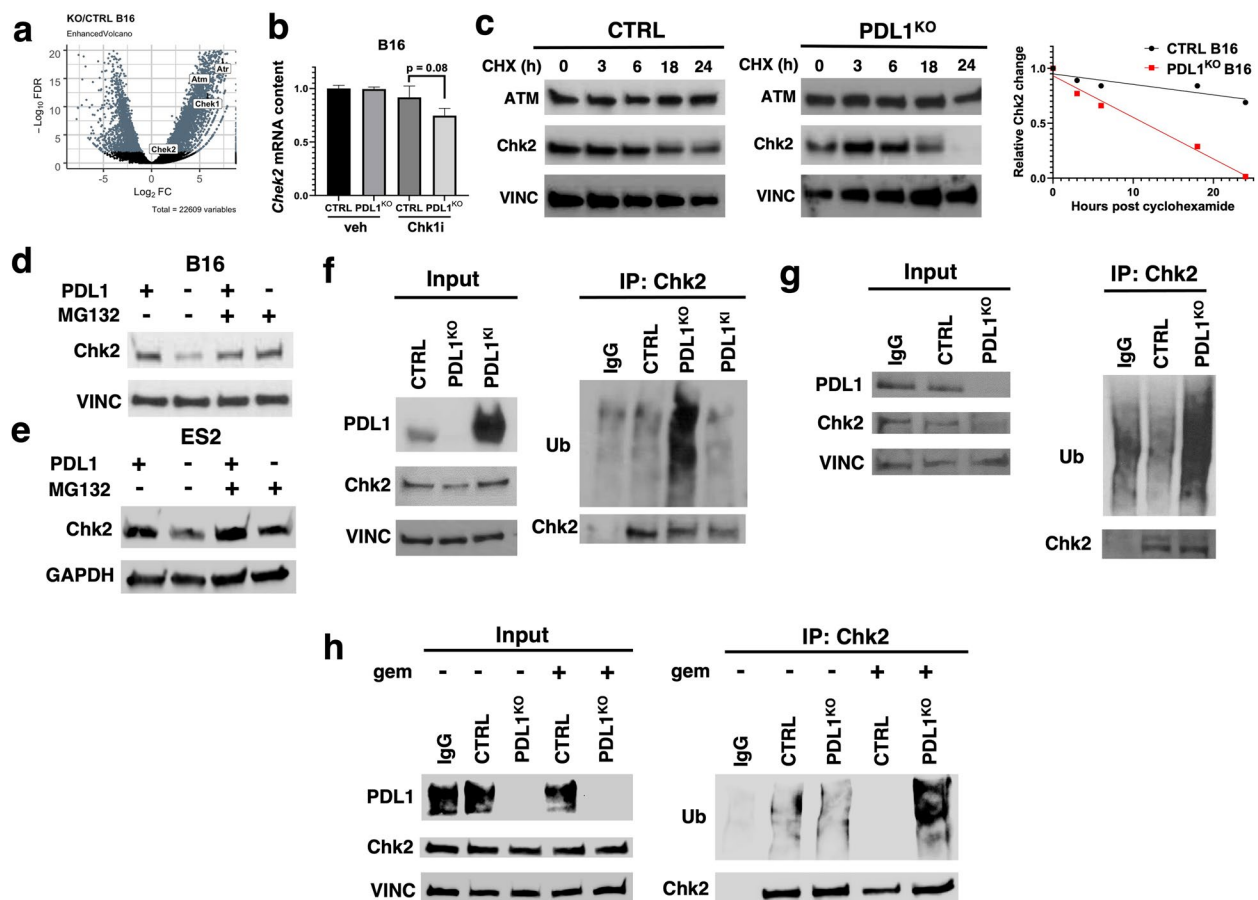


Fig. 6 PDL1 protects Chk2 from ubiquitination in distinct tumours. **a.** Volcano plot of RNA-seq data depicting PDL1^{KO} effect on select mRNA levels versus CTRL B16. **b.** qRT-PCR of *Chk2* mRNA in CTRL versus PDL1^{KO} B16 cells treated with DMSO or rabusertib. *P*, unpaired *t*-test. **c.** Immunoblot of CTRL versus PDL1^{KO} B16 cells treated with cycloheximide (CHX). Summary graph depicts normalised total Chk2 protein levels quantified using ImageJ. **d.** Immunoblot of CTRL versus PDL1^{KO} B16 and **e.** ES2 cells treated with MG132 (2 μ M) for 12-h. **f.** Immunoblot of immunoprecipitated Chk2 from CTRL, PDL1^{KO}, and stable PDL1 knock-in (PDL1^{KI}) B16 cells and **g.** CTRL and PDL1^{KO} ES2 cells after MG132 treatment. **h.** CTRL and PDL1^{KO} T24 cells treated with MG132 for 16-h plus vehicle (H₂O) or 10 ng/mL gemcitabine (gem). Endogenous Chk2 was immunoprecipitated and Chk2 and ubiquitination (Ub) were detected by immunoblot

Ubiquitination is a major post-translational modification regulating DDR protein availability [39]. We treated CTRL and PDL1^{KO} B16 and ES2 cells with the proteasome inhibitor MG132, which restored Chk2 expression in PDL1^{KO} B16 and ES2 cells to CTRL levels (Fig. 6d-e). PDL1^{KO} B16 cells exhibited significantly elevated ubiquitinated Chk2, while stable PDL1 re-expression (PDL1^{KI}) into PDL1^{KO} cells completely reversed Chk2 ubiquitination (Fig. 6f). Baseline Chk2 ubiquitination in PDL1^{KO} versus CTRL ES2 cells was similarly high (Fig. 6g), consistent with their decreased basal Chk2. PDL1^{KO} T24 cells only exhibited increased Chk2 ubiquitination after DNA damage induction with gemcitabine (Fig. 6h), supporting observed total Chk2 deficiency only after DNA damage induction. These

data fully accord with tumour PDL1 protection of Chk2 from ubiquitination and subsequent proteasome-dependent degradation in multiple murine and human tumour models.

PDL1 protects Chk2 from PIRH2-mediated ubiquitination and degradation

As both mouse and human PIRH2, an E3 ligase, can regulate Chk2 ubiquitination and degradation basally or upon DNA damage [39], we hypothesised that tumour-intrinsic PDL1 could interfere with PIRH2 E3 ligase regulation of Chk2. We depleted PIRH2 in CTRL or PDL1^{KO} B16 or PDL1⁺ NCH1 and PDL1⁻ NFH1 *Nras*^{Q61R} cells and found that PIRH2 depletion fully rescued Chk2 expression in PDL1^{KO} B16 and PDL1⁻ NFH1 cells versus

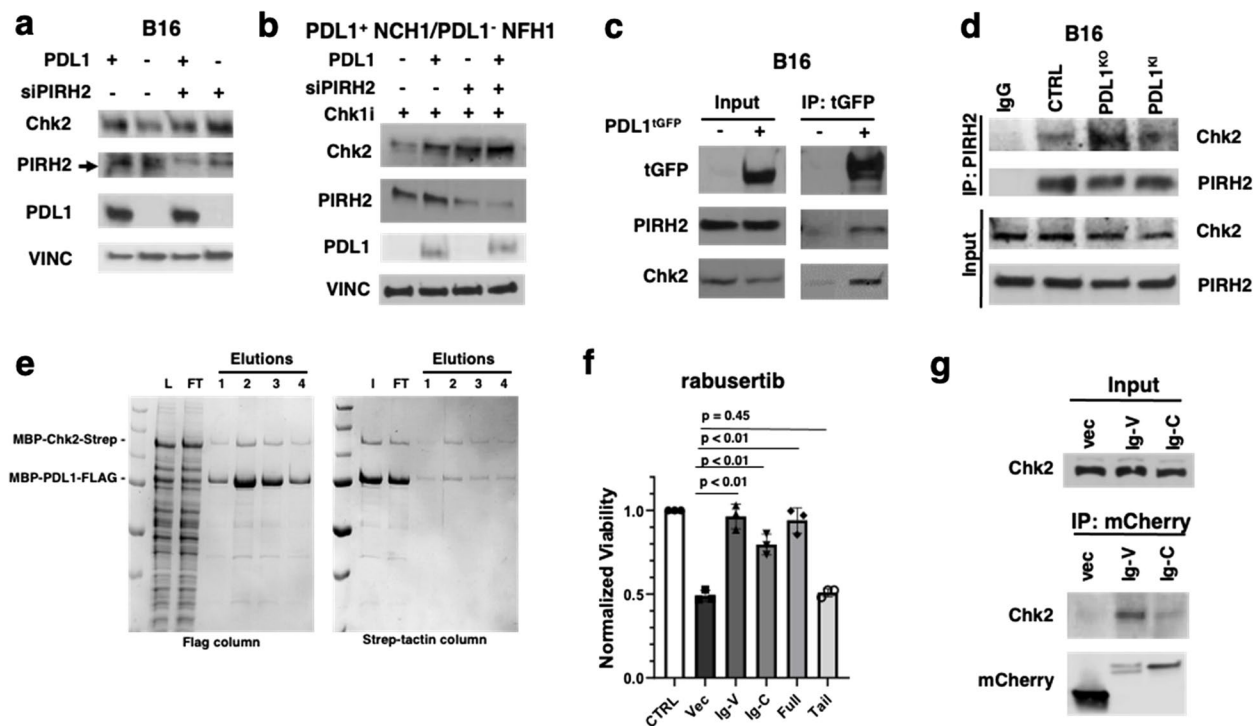


Fig. 7 Tumour PDL1 protects Chk2 from PIRH2 E3 ligase-mediated degradation in distinct tumours through its immunoglobulin-like domains. **a.** Non-targeting or PIRH2-specific siRNA vectors transfected into CTRL or PDL1^{KO} B16 cells or **b.** PDL1⁺ NCH1 cells and PDL1⁻ NFH1 cells. **c.** Interaction among PDL1, Chk2 and PIRH2 in B16 cells stably expressing vector control or turbo-GFP (tGFP)-tagged PDL1 (PDL1^{IGFP}) treated with MG132 and co-immunoprecipitated with tGFP trap beads followed by immunoblotting. **d.** Endogenous PIRH2 co-immunoprecipitated in CTRL, PDL1^{KO}, and PDL1^{KI} B16 cells. **e.** Left: Flag-tagged human PDL1 and Streptavidin-tagged human Chk2 were co-expressed in Tni cells and affinity pull-downs of lysates with Flag resin and eluate fractions (1,2,3,4) followed by SDS-PAGE and Coomassie blue staining. Right: eluates were pooled for reciprocal Chk2 affinity pull-down using Strep-tactin resin. L, lysates; FT, flow-through; I, input. **f.** Viability of PDL1 truncation mutant-expressing B16 cells 72-h post rabusertib (2.5 μ M) treatment. *P*, unpaired *t*-test. **g.** Immunoblot of domain-expressing B16 cells immunoprecipitated using anti-mCherry beads

respective CTRL cell line levels (Fig. 7a-b). PDL1 depletion did not significantly alter PIRH2 content and PIRH2 knockdown did not alter PDL1 content. We also depleted MDM2 in B16 cells, another E3 ligase controlling Chk2 protein content in selected cells, but Chk2 was unaffected (Fig. S8a). Nonetheless, these data do not fully exclude a role for MDM2 in controlling PDL1-regulated Chk2 content.

PDL1, PIRH2, and Chk2 formed a single complex in B16 cells by co-immunoprecipitation (Fig. 7c), suggesting that PDL1 could directly interfere with PIRH2-mediated Chk2 degradation. PIRH2 binding to Chk2 was significantly increased in PDL1^{KO} B16 cells and was rescued to CTRL levels in PDL1^{KI} cells (Fig. 7d). Since Chk2 is largely nuclear, we asked whether PDL1 could co-localise with Chk2 in nuclei to modulate its ubiquitination. First, we validated nuclear PDL1 content in B16 cells by sub-cellular fractionation and immunoblotting (Fig. S8b). We observed nuclear PDL1-Chk2 co-localisation in B16 cells (Fig. S8c) and confirmed a PDL1-Chk2 interaction biochemically by co-expressing recombinant FLAG-tagged PDL1 and Streptactin-tagged Chk2 in Tni cells (Fig. 7e),

demonstrating that PDL1 and Chk2 co-purify, consistent with direct protein–protein interaction. These data collectively support that PDL1 physically antagonises the interaction between the PIRH2 E3 ligase and Chk2, including in the nucleus, thus preventing ubiquitin-mediated Chk2 degradation and facilitating Chk2 protein stability. These data are consistent with prior reports of functional nuclear PDL1 [33].

PDL1 IgV and IgC domains control Chk2 protein content and Chk1i resistance

We generated mCherry-tagged fragments of PDL1 from aa18-132, aa133-220, and aa260-290 (Fig. S9a) corresponding to Ig-V-like, Ig-C-like, and C-terminal (cytoplasmic) tail domains, respectively [9]. These constructs lack both the PDL1 signal peptide and transmembrane domains and therefore are not membrane-bound and cannot be surface-expressed. We re-expressed them or controls individually in PDL1^{KO} B16 cells and validated PDL1 fragment expression (Fig. S9b). Chk1i resistance was fully restored by re-expression of full-length PDL1, PDL1 Ig-V domain, partially by the Ig-C domain, but

not by the 30aa C-terminal tail (Fig. 7f). Consistent with these data, Chk2 interacted strongly with the PDL1 Ig-V N-terminal domain and slightly with the Ig-C N-terminal domain by co-immunoprecipitation (Fig. 7g), suggesting the PDL1 Ig-V domain could predominantly interact with Chk2 to prevent its ubiquitination. These data are also together consistent with fully intracellular PDL1 controlling Chk1i resistance through its N-terminal domains, as our PDL1 domain constructs are fully intracellular, and support our PDL1^{cyto} data.

Pharmacologic tumour PDL1 depletion phenocopies genetic PDL1 knockout in eliciting Chk2 depletion and Chk1i synthetic lethality

α PDL1 and α PD1 immune checkpoint blockade is now being tested in clinical trials combined with DDRi, but such combinations have thus far failed to demonstrate convincing efficacy. Strategies to overcome DDRi and immune checkpoint blockade treatment resistance remain obscure. We found that α PDL1 treatment does not deplete tumour PDL1 or Chk2 or improve γ H2AX induction with Chk1i in B16 cells in vitro (Fig. S10a). The role of tumour-intrinsic PDL1 signals in the ATM/Chk2 pathway and Chk1i treatment responses prompted us to identify pharmacologic agents targeting total tumour cell PDL1 content versus surface PDL1 alone. We recently identified FDA-approved drugs that could be repurposed as PDL1-depleting drugs, including the β -lactam cephalosporin antibiotic cefepime [15], but its effects on Chk2 are not reported. Cefepime alone specifically depleted Chk2 protein in B16 cells under conditions in which it significantly depletes PDL1 [15] but depleted Chk2 in T24 cells only when combined with rabusertib (Fig. S10b, Fig. 8a), replicating the DNA damage-dependent, PDL1-dependent control of tumour Chk2 content seen with genetic PDL1 depletion in T24 cells. While cefepime depleted Chk2 in CTRL B16 cells, it did not significantly deplete Chk2 in PDL1^{KO} B16 or PDL1^{KI} B16 that significantly and stably overexpressed PDL1 (Fig. 8b). Though cefepime alone did not affect cell

viability, it potently induced synthetic lethality with rabusertib in MDA-MB-231 and T24 cells (Fig. 8c-d) as also elicited by genetic PDL1 depletion. Notably, cefepime did not enhance rabusertib synthetic lethality in PDL1^{KO} T24 cells (Fig. 8e), confirming PDL1 dependency of cefepime-mediated Chk1i synthetic lethality. Rabusertib sensitivity elicited by cefepime was essentially equivalent to full genetic PDL1^{KO} (Fig. S10c). Cefepime did not affect ATR or Chk1 content in B16 and T24 cells (Fig. S10d-e), again phenocopying genetic PDL1^{KO}.

Unlike conventional cytotoxic chemotherapy, cefepime is not a known DNA-damaging agent outside of our recent report and another that suggested certain cephalosporins have radio-sensitising capabilities [15, 40]. We therefore considered a potential β -lactam class effect on enhancing Chk1i synthetic lethality and compared several β -lactam drugs representing different subclasses. The β -lactam ceftazidime shared similar molecular moieties with cefepime, including a quaternary ammonium group (green) and an oxime-aminothiazole group (purple, Fig. S10f). Previously, we showed that ceftazidime depletes tumour PDL1 [15]. Ceftazidime also reduced Chk2 expression in B16 cells as a single agent under conditions in which it significantly depletes PDL1 [15] (Fig. S10g) and in T24 cells combined with rabusertib (Fig. 8f). Ceftazidime did not deplete Chk2 in PDL1^{KO} or PDL1^{KI} B16 compared to CTRL B16 (Fig. 8g), similarly to cefepime and consistent with PDL1 dependence of ceftazidime-mediated Chk2 depletion. Ceftazidime but not structurally distinct β -lactams cefazolin, meropenem, penicillin G, or ceftriaxone sensitized PDL1⁺ CTRL T24 tumour cells to the Chk1i rabusertib in a PDL1-dependent manner (Fig. 8h-k). Thus, the ability to sensitize tumour cells to Chk1i is a feature of specific β -lactams and not a class effect. Ceftazidime elicited rabusertib sensitivity similar to genetic PDL1^{KO} in T24 cells (Fig. S10h). Ceftazidime also did not affect ATR/Chk1 content in B16 cells or T24 cells (Fig. S10i-j), further consistent with genetic PDL1 depletion. Ceftazidime sensitized PDL1⁺ NCH1 tumours to Chk1i in vivo, (Fig. 8l-m), similarly to cefepime [15],

(See figure on next page.)

Fig. 8 Pharmacologic tumour PDL1 depletion replicates genetic tumour PDL1^{KO} by depleting Chk2 and inducing Chk1i synthetic lethality.

a. Immunoblot of CTRL T24 cells for indicated proteins after 72 h of treatment with vehicle (DMSO), 1 μ M rabusertib (Chk1i), 80 μ M cefepime, or combination. **b.** Immunoblot of CTRL, PDL1^{KO}, and stable PDL1^{KI} B16 cells treated with 80 μ M cefepime for indicated time points. **c-e.** Cell viability of **c.** CTRL MDA-MB-231, **d.** CTRL T24, and **e.** PDL1^{KO} T24 cells treated with indicated concentrations of rabusertib \pm 80 μ M cefepime or vehicle (DMSO) for 96 h. *P*, two-way ANOVA. **f.** Immunoblot of CTRL T24 cells treated with vehicle, 1 μ M rabusertib, 80 μ M ceftazidime, or both for 72 h. **g.** Immunoblot of CTRL, PDL1^{KO} and stable PDL1^{KI} B16 cells treated with 80 μ M ceftazidime for indicated time points. **h-j.** Cell viability of **h.** CTRL MDA-MB-231, **i.** CTRL T24, and **j.** PDL1^{KO} T24 cells treated with indicated concentrations of rabusertib \pm 80 μ M ceftazidime or vehicle for 96 h. *P*, two-way ANOVA. **k.** MTT viability analysis of CTRL T24 cells treated for 96 h with 80 μ M of indicated β -lactams with rabusertib. *P*, two-way ANOVA. **l.** Growth curves of PDL1⁺ NCH1 tumours implanted subcutaneously in WT mice treated with vehicle, ceftazidime, rabusertib, or both. *P*, two-way ANOVA. **m.** Tumour weights of NCH1 tumours from **l.** at endpoint (day 18). *P*, unpaired *t*-test. Vehicle (veh), ceftazidime (ctz), rabusertib (rab), and ceftazidime + rabusertib (combo) groups are indicated

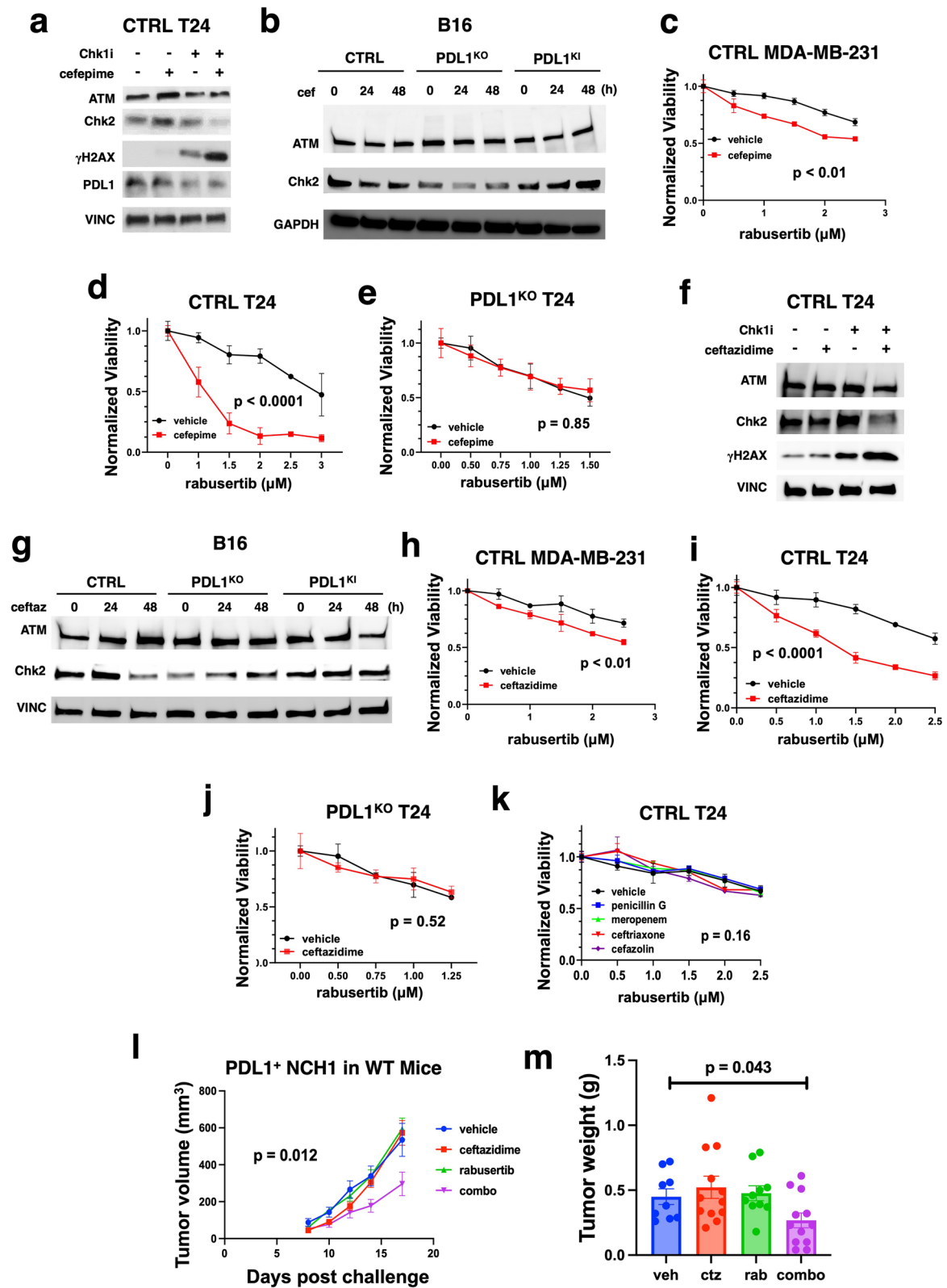


Fig. 8 (See legend on previous page.)

highlighting the clinical therapeutic potential of targeting tumour-intrinsic PDL1 signals with distinct PDL1 depletion drugs.

Discussion

Here, we show that tumour-intrinsic PDL1 specifically regulates the Chk2 DDR signaling pathway by preventing Chk2 ubiquitin-mediated degradation and suppressing Chk1 efficacy (Fig. S11). Although PDL1 regulates Chk2 protein stability but also DDR protein transcripts, these distinct mechanisms of DNA damage regulation could overlap in certain instances, requiring further investigation. Our biochemical and genetic studies showed that tumour-intrinsic PDL1 can form protein complexes with Chk2 and co-localise with Chk2 in cellular nuclei, where the DNA damage response is initiated to prevent Chk2 ubiquitination. Tumour-intrinsic PDL1 control of specific molecular interactions and post-translational gene product expression through protein ubiquitination provide new mechanistic bases to explain the diverse pathologic consequences driven by tumour-intrinsic PDL1. As E3 ligase activity varies among cells and as other E3 ligases promote Chk2 polyubiquitination, PDL1 could protect from other E3 ligases to inhibit Chk2 ubiquitination in other cell types.

We showed that intracellular tumour PDL1 mediates Chk2 protein control and Chk1 synthetic lethality while membrane-bound PDL1 promoted distinct outcomes, including epithelial-to-mesenchymal transition. Others previously reported that subcellular tumour PDL1 mediates important pathologic signals almost exclusively through its C-terminal tail [9]. In contrast, we identified PDL1 regions outside of the C-terminal tail that support Chk2 protein content and Chk1 resistance. Additional work is required to define further mechanistic details, including the precise subcellular location where PDL1-controlled Chk2 content control occurs and other tumour-intrinsic signaling outcomes of specific PDL1 domains. Nonetheless, subcellular tumour PDL1 location could be a treatment response biomarker for DNA damaging agents.

The important anti-tumour cytokines IFN γ and TNF α increase surface membrane PDL1 expression that inhibits anti-tumour immunity, termed adaptive resistance [2], but neither induced significant tumour cytoplasmic PDL1 accumulation in a study of that effect [34]. We found that both cytokines preferentially increased tumour surface PDL1 content rather than non-surface PDL1 and did not reverse Chk1 synthetic lethality, consistent with our demonstration of the importance of non-surface PDL1. Lack of Chk1 synthetic lethality reduction by these cytokines that potently induce PDL1 could be a function of insufficient non-surface PDL1 induction,

near-maximal basal Chk1 resistance of these tumour cells, or unknown mitigating cytokine effects. As both cytokines only minimally induce nuclear PDL1 [34], and we identified the cytoplasm as a key non-surface location for PDL1 effects we describe, further work is needed to define specific contributions from specific non-surface locations.

Despite some pre-clinical studies showing increased DDRi efficacy when combined with PDL1/PD1 in tumours with presumed underlying DNA repair defects [41], this strategy appears incompletely effective in cancer patients [42]. We showed robust synthetic lethality to Chk1 in multiple human and mouse immune checkpoint blockade-resistant tumour models (*e.g.*, 4T1 [16], ID8agg [43]) following genetic PDL1 knockout in vitro and in vivo without immune contributions. Our in vivo Chk1 dosing was highly successful at inhibiting in vivo tumour growth of various PDL1-deficient tumours, suggesting that efficacy could be improved when tumour PDL1 status is taken into consideration, which could serve as a DDRi response biomarker. Reduced PDL1-dependent Chk2 expression during the DDR was sufficient for robust Chk1 synthetic lethality in some tumour cells, but only partial reversal of Chk1 sensitivity following Chk2 re-expression in PDL1^{KO} T24 cells implicates additional mechanisms for tumour PDL1-dependent Chk1 synthetic lethality and likely Chk2 control. These differences in Chk2 dependency for synthetic lethality with Chk1 likely relate to tissue-specific signaling and to distinct mutational landscapes in different tumour cells, among other considerations. Other DDR protein inhibitors involved in DNA replication and repair such as ATM, Wee1, and DNA-PK are also in clinical trials [44, 45], which could address some of these additional factors. Notably, cell proliferation rate tends to correlate with DDRi efficacy [46], whereas in the case of genetic or pharmacologic PDL1 depletion, we find that cells generally tend to proliferate more slowly despite increased sensitivity to these agents [9, 16]. These data underscore the complexity and as-yet unknown details of the DDR. Full definition of these complex mechanisms will continue to enhance our ability to improve treatments. Additionally, compared to rabusertib, prexasertib is more potent at inhibiting Chk1 and inducing growth arrest [47]. Increased efficacy of prexasertib versus rabusertib in PDL1^{KO} B16 cells (Fig. 2a and Fig. S2d) might also be due, at least in part, to the differential potencies of distinct small molecule inhibitors. Additionally, some ATR substrates could antagonize Chk2 function [48, 49], which adds another layer of complexity to their interactions and effects in cellular pathways. Finally, the Chk1 UCN-01 induced significantly more γ H2AX than ATRi [48], leading some to conclude that inhibition of Chk1 is more

deleterious to cycling cells than inhibition of ATR [49, 50], which could help explain increased Chk1i efficacy versus ATRi efficacy in distinct PDL1^{KO} tumour cells.

DNA damage induces cytosolic DNA, which can activate RNA or DNA pattern recognition receptors and subsequent type-I interferon signaling [9]. Thus, intact DNA damage checkpoints in tumour cells are crucial in preventing activation of these receptors and avoiding anti-tumour immunity [9]. Previously, we showed that PDL1 deficiency increases STING signals when combined with the PARP inhibitor olaparib [16], and genetic [16] or pharmacologic tumour PDL1 depletion with cefepime or ceftazidime [15] activates immunogenic tumour STING signals, which could be a result of deficient DDR and could improve immune-dependent treatments [51]. Here, we show that in vivo Chk1i induces specific anti-tumour immune populations specifically in PDL1^{KO} tumours, including granzyme B-producing CD8⁺ T cells and NK cells, which could be a result of increased tumour immunogenicity from DNA damage and subsequent cGAS/STING activation. Further, Chk1i efficacy in B16 and NCH1/NFH1 models in vivo is immune dependent, specifically requiring adaptive immunity in PDL1^{KO} B16 tumours, supported by increased CD8⁺ T cells in the tumour microenvironment. Our immune profiling data from PDL1-deficient B16 and NFH1 tumours ex vivo show decreased prevalence of accepted anti-tumour immune populations, including CD8⁺ T cells in NFH1 tumours, yet their prevalence increased with Chk1i. Thus, further work into the influence of tumour-intrinsic PDL1 on the tumour immune microenvironment with DNA damage and CD8⁺ T cell control of PDL1^{KO} tumours from Chk1i treatment is warranted.

Treatment efficacy in PDL1^{KO} but not CTRL tumours could owe in part due to the known increased PDL1 with DNA damage [9], which could be overcome with our pharmacologic tumour PDL1 depletion strategy. Pharmacologic tumour PDL1 depletion could also augment combinations using cytotoxic DNA damaging agents, which usually increase tumour PDL1 [16]. Further investigation into tumour-intrinsic, immune checkpoint-independent PDL1 effects on tumour immune evasion and immune modulators, including regulation of the DNA damage response and suppression of type-I interferon signals post-DNA damage, could define additional roles for tumour-intrinsic PDL1 in cancer pathogenesis and improve immunotherapy responses.

Targeting tumour-intrinsic PDL1 signals through genetic and pharmacologic tumour PDL1 depletion improves various cancer treatments, including cytotoxic chemotherapy and immune checkpoint blockade [12–15]. Our data suggest that depleting the intracellular PDL1 pool with PDL1 depleting drugs could be an

effective strategy to increase DDRi treatment response compared to surface PDL1 targeting with available immune checkpoint blockade agents. The cephalosporin antibiotics cefepime and ceftazidime deplete tumour PDL1 to phenocopy genetic PDL1 knockout effects on Chk2 protein and sensitize tumour cells to Chk1i. Cephalosporins are not reported to affect specific DDR signals, but the cephalosporin cephalixin sensitized tumour cells to ionizing radiation, a double strand break-inducing agent [40]. Other β -lactam antibiotics, including alternative cephalosporins that we tested, did not induce synthetic lethality with Chk1i, suggesting there is not a cephalosporin or β -lactam class effect to deplete PDL1, impair the ATM/Chk2 DNA damage response, or sensitize to Chk1i. Additionally, cefepime and ceftazidime suppress PDL1 expression under DNA damage conditions. Thus, our pharmacologic tumour PDL1 depletion approach could be applied to genotoxic agents to overcome the potential decrease in efficacy due to increased PDL1 expression with DNA damage. Our data support the use of PDL1-depleting agents such as cefepime as adjunct therapy to Chk1i and have rapid translational potential.

Conclusions

We identified a novel function of tumour-intrinsic PDL1 in promoting the Chk2 DNA damage response, Chk1i resistance, and regulating DDR protein ubiquitination in human and mouse cell lines, an autochthonous melanoma model, and in primary human tumour cells. We identified novel roles for membrane versus intracellular PDL1 in modulating different tumour-intrinsic PDL1 signals and replicated genetic phenotypes with pharmacologic tumour PDL1 depleting drugs cefepime and ceftazidime, demonstrating their relevance as a novel therapeutic strategy with rapid clinical translation potential. Understanding tumour PDL1 contributions to the DDR provides important insights into tumour PDL1-driven pathogenesis and mechanisms underlying DDRi treatment resistance.

Methods

Chemicals and reagents

Rabusertib (S7109), prexasertib (S7178), AZD0156 (S8375), ceftazidime (S3649), and AZD6738 (S7693) were purchased from Selleckchem. MG132 (474,790), cycloheximide (0180), cefepime for in vitro studies (A3737), gemcitabine (G6423), and 4-hydroxytamoxifen (H6278) were purchased from Sigma-Aldrich. Human and mouse recombinant interferon-gamma (IFN γ , 485-MI, 285-IF) and TNF-alpha (TNF α , 410-MT, 210-TA) were from R&D Systems. BML-277 (HY-13946), Pifithrin- α (HY-15484) and nutlin-3a (HY-10029) were

purchased from MedChem Express. AZD0156 was dissolved in ethanol, and gemcitabine and ceftazidime were dissolved in water. Penicillin G, meropenem, ceftriaxone, and cefazolin were obtained from Oakdell Pharmacy (7220 Louis Pasteur Dr., San Antonio, TX, 78,229) and dissolved in sterile 0.9% NaCl. Remaining drugs used for in vitro drug studies were dissolved in dimethyl sulfoxide (DMSO). Drugs were aliquoted in individual tubes, stored at -80°C , and thawed as needed to avoid multiple freeze-thaws or made fresh when required. The α PD1 antibody pembrolizumab was purchased from Invivogen, and the α PD1 antibody balstilimab was a kind gift from Agenus. The α -mouse PDL1 antibody (clone 10F.9G2) and IgG isotype control were purchased from BioXCell (BE0101, BE0090). In vivo ceftazidime was from MedChem express.

Cell lines

B16-F10 (herein B16), ID8agg, ES2, and 4T1 we described previously [10, 13]. All of these cell lines were grown in RPMI-1640 containing 5% fetal bovine serum, 1% penicillin/streptomycin, 1% L-glutamate, and 1% HEPES buffer (Gibco, ThermoFisher, “complete medium”). T24 cells were a gift from R. Svatek (UTHSA) and cultured in McCoy’s 5A complete medium (Thermo-Fisher). PDL1⁻ *TN^{6IR}* and PDL1⁺ *TN^{6IR}* Nras mutant mouse melanoma cells (NFH1 and NCH1 respectively) were made from single cell suspensions of tumours from 4-hydroxytamoxifen-induced mice plus UVB (4.5 kJ/m²) and passaged in vitro as polyclonal cell populations. NCH1, NFH1, MDA-MB-231, and Tni cells were grown in DMEM complete medium. All cell lines were periodically tested by Mycoalert PLUS (Lonza Bioscience) and confirmed *Mycoplasma*-free.

Stable PDL1^{lo} cell lines were generated using shRNAs targeting *CD274* or non-targeting controls as we previously described [10]. B16 cells were infected with lentivirus expressing murine control or Raptor-targeting shRNAs from Sigma-Aldrich (TRCN0000077469) and transduced cells were selected in 2 mg/mL neomycin to generate Raptor^{lo} cells. PDL1^{KO} T24 cells were generated by CRISPR/Cas9 as we previously described [25] and PD1^{lo} T24 by using lentiviral particles containing *PDCDI* shRNAs (TRCN0000083508) from Sigma-Aldrich. PD1^{KO} and PDL1^{KO} B16 cells were generated using CRISPR/Cas9-GFP expression plasmids (SantaCruz Biotechnology), which included 3 pooled sgRNAs targeting PD1 or PDL1. sgRNA sequences used for CRISPR/Cas9 mediated gene deletion for PD1 were (1) 5'-AGCCCC TCGCCCAAACCAGA-3'; (2) 5'-CGGAGGATCTTA TGCTGAAC-3'; 5'-GTGCCTCGGCCATGGGACGT-3'. sgRNA sequences for PDL1 were (1) 5'-GTATGGCAG CAACGTCACGA-3'; (2) 5'-CTGGATCCACGGAAA

TTCTC-3'; (3) 5'-TCCAAAGGACTTGTACGTGG-3'. Stable PDL1^{KI} B16 was generated as previously described [10]. Plasmids were transfected using Turbofect reagent (Thermo-Fisher) according to the manufacturer’s protocol. Cells were cytometrically sorted by GFP expression, then single cell clones were isolated and analysed for targeted gene disruption using genomic DNA PCR primers spanning exon regions of PD1 or PDL1. Gene targeting was validated by Immunoblotting and/or sequencing.

Plasmids, transfections, and lentivirus transductions

Chk2 expression plasmids or vector only controls for Chk2 re-expression experiments (Chk2^{RE}) were obtained from OriGene (RC201278 and MR208692 for human and mouse, respectively). RCHY1 (PIRH2) siRNA Smartpools or scrambled controls were obtained from Dharmacon (Cat#: L-065323-01-0005). Mouse PDL1 expression plasmid for rescue experiments and further subcloning was from OriGene (Cat#: MG203953). Transient transfections were performed using lipofectamine 3000 reagent (Thermo-Fisher) per the manufacturer’s protocol. Transient induction of differential PDL1 expression into PDL1^{KO} ES2 cells by was by transfecting empty vector (Addgene 72299) or human Flag-PDL1 (Addgene 121446) expression plasmids. After 48-h, cells were collected and lysed for immunoblot analysis.

For PDL1^{mem} expression constructs, a mouse PDL1-tGFP fusion protein construct (OriGene MG203953) was PCR amplified and subcloned into the pDisplay vector (Invitrogen) at the BglII and PstI sites, resulting in N-terminal fusion to the murine Ig κ -chain leader sequence and C-terminal fusion to the platelet derived growth factor receptor transmembrane domain, anchoring PDL1 to the extracellular plasma membrane (PDL1^{mem}). To generate intracellular localised PDL1 constructs (PDL1^{cyto}), a myristoylation (myr) tag [52] was incorporated at the N-terminus of PDL1, preventing PDL1 from extracellular surface presentation. To generate the pcDNA-myr-PDL1^{cyto} expression vector, mouse PDL1-GFP CDS was PCR amplified and cloned into a pcDNA6C vector (Invitrogen) using EcoRI-XhoI sites. All constructs were sequence verified.

PDL1 vectors with C-terminal mCherry tag (pLV-mPDL1 aa18-132-mCherry, pLV-mPDL1 aa133-220-mCherry, pLV-mPDL1 aa1-260-mCherry, pLV-mPDL1 aa1-290-mCherry, pLV-mPDL1 aa260-290-mCherry) were designed using pLV-mCherry-vector backbone and were custom synthesized and sequence verified by Vector Builder (Chicago, IL). All PDL1 mutant constructs were CRISPR/Cas9 resistant for stable re-expression in PDL1^{KO} cells.

Lentivirus was produced by transfecting HEK293T cells with targeting plasmid along with packaging

vectors pMD-2G, pMDLg/pRRE and pRSV-Rev plasmids (Addgene 12259, 12,253, 12,251) using Turbofect Transfection Reagent (R0531, Thermo Scientific) according to the manufacturer's transfection protocol. The lentivirus-containing supernatants were collected 24 and 48 h after transfection and concentrated by concentrator (Lenti-X, cat 631,231, Takara). Transduction was performed by adding the lentivirus to PDL1^{KO} B16 cells in the presence of polybrene (10 µg/mL, TR-1003-G, Sigma), followed by selection with puromycin (1 µg/mL) for 14 days. Similarly, PDL1^{KO} B16 cells stably expressing pDisplay-PDL1^{mem} and pcDNA-myr-PDL1^{int} constructs were generated by neomycin selection (2 mg/mL). Pooled clones were selected and expression of recombinant proteins was confirmed by immunoblotting and/or imaging as indicated.

Immunoblots and subcellular fractionations

Immunoblotting was performed as we described [53, 54]. Briefly, cells were lysed using RIPA buffer (20 mmol/L Tris-HCl, pH 8.0, 150 mmol/L NaCl, 1 mmol/L disodium EDTA, 1 mmol/L EGTA, 2.5 mmol/L sodium pyrophosphate, 1 mmol/L β-glycerophosphate, 1% triton-X100 plus Halt protease/phosphatase inhibitor cocktail from Thermo-Fisher (78,442). Plasma membrane/subcellular fractionation kit was obtained from Abcam (ab65400). Protein concentrations were quantified using a Pierce-BCA Kit (23,328). 20–40 µg of lysate plus 4×loading dye were run on 4% to 15% gradient SDS-PAGE Precast TGX gels (Bio-Rad) and transferred to nitrocellulose membranes (Bio-Rad) using a rapid transblot system (Bio-Rad). Membranes were blocked in TBS (pH 7.4) plus 1% Tween-20 (TBST) and 5% non-fat dry milk, incubated overnight at 4° C with diluted primary antibodies against indicated proteins. Membranes were incubated with either horseradish peroxidase-conjugated secondary antibodies (Cell Signaling) for 2 h at room temperature then washed with TBST 3 times for 3 min each followed by incubation with Western Lightning Plus ECL reagent from Perkin Elmer (NEL10400L). ImageJ or ImageLab softwares were used to quantify relative band intensity by normalizing to loading controls. Antibodies against the following targets from Cell Signaling were used: PDL1 (#13,684), ATM (#2873S), Vinculin (#18799S), γH2AX^{ser139} (#9718S), Chk2 (#2662S), GAPDH (#2118S), Ubiquitin (#58395S), Rabbit HRP-conjugated secondary (#7074S), Mouse HRP-conjugated secondary (7076S), p-ATR^{Ser428} (#2853S), p-Chk1^{ser345} (#2348S), ATR (#13934S), p-Chk2^{Thr68} (#2197S), p-ATM^{Ser1981} (#5883S), Na⁺/K⁺ ATPase (#3010S), PDL1 (#29122S), Chk1 (#2360S), Vimentin (#3932S), Chk2 XP (#6334S), and Chk2 (3440S). Antibodies from Abcam against these targets were: PDL1 (ab213480) and PIRH2

(ab189907). Antibodies from Santa Cruz include those detecting Chk2 (sc-5278) and PIRH2 (sc-374505). The detection antibody against PD1 was from Thermo-Fisher (7A11B1), and RFP detection antibody (dsRED polyclonal) was from Takara (632496). Primary and secondary antibody dilutions were made per the manufacturer's recommendation. Membrane and cytoplasmic fractionations were performed using the plasma membrane protein extraction kit (Abcam ab65400) following manufacturer's instructions. Membrane fraction is pure surface plasma membrane. Cytoplasmic and nuclear fractionations were performed using NE-PER nuclear and cytoplasmic extraction reagents (Thermo Scientific 78833).

Immunoprecipitation

Cells were cultured on 15-cm² plates, trypsinized, and counted with Vi-Cell XR cell viability analyzer with 10 million cells used per immunoprecipitation sample. After centrifugation at 500×gravity for 5 min, cell pellets were washed with ice-cold 1×PBS and lysed in Pierce IP Lysis Buffer (#87,787) supplemented with 1:100 Halt Protease and Phosphatase Inhibitor Cocktail (#78,442) from Thermo-Fisher. Samples were incubated on a rotator for 15 min at 4° C then centrifuged at 13,000×gravity for 15 min at 4° C. Supernatants were transferred to a new microcentrifuge tube. Input fractions were transferred to a new tube and boiled with equivalent volume of 2×loading dye for 10 min. Antibodies against Chk2 (sc-5278), PIRH2 (sc-374505), or normal mouse IgG (sc-2025) as indicated for endogenous protein pull-downs were added to the remainder of the supernatants and incubated on a rotator overnight at 4° C. Pierce Protein G Magnetic Beads (Thermo-Fisher) were washed with ice-cold 1×PBS four times on a magnetic rack, resuspended in Pierce IP Lysis Buffer, and added to immunoprecipitation samples. For co-immunoprecipitation of mCherry or turbo-GFP (tGFP) tagged PDL1 recombinant proteins, we used pre-conjugated RFP or tGFP trap beads (Chromotek). Samples were incubated on a rotator for 2 h at 4° C then washed four times with ice-cold 1×PBS on a magnetic rack. Beads from each immunoprecipitation sample were resuspended in 1×loading dye and boiled for 10 min, and supernatants were transferred to a new tube. Samples were subsequently analyzed via immunoblotting as described above.

RT-qPCR

CTRL or PDL1^{KO} cells were harvested with vehicle controls or rabusertib and subjected to total RNA extraction using TRIzol reagent. A Superscript Vilo kit (Invitrogen) was used for reverse transcription of total RNA followed

by qPCR of cDNAs using the SYBR green method. The following primers were used for murine *Chk2*: 5'- CCG AGCTTATTGGGAAAGGC-3'; 5'- AGCCATCTTTAC CTCCCCAC -3' and *β-Actin*: 5'- CATTGCTGACAG GATGCAGAAGG -3'; 5'- TGCTGGAAGGTGGAC AGTGAGG-3'. Data were analyzed by the $2(-\Delta\Delta C(T))$ method.

In vitro viability assays

Tumour cells were seeded in a 96 well plate. B16 and ID8agg cells were seeded into 96 well plates pre-coated with fibronectin derived from bovine plasma (Sigma Aldrich). All cells were treated with indicated drugs and respective vehicle controls for the indicated time periods. Plates were then incubated with 3-(4,5-dimethylthiazolyl-2)-2,5-diphenyl tetrazolium bromide (MP Bio) MTT reagent (3 mg/ml) for 2 h. Medium was fully decanted and 200 μ l of DMSO was added to each well. Plates were read at 490 nm with a BIO-TEK Synergy HT plate reader. Raw data was analyzed using Excel and normalized data plotted using Graph Pad Prism software. Cefepime, ceftazidime, penicillin G, meropenem, ceftriaxone, and cefazolin were used at 80 μ M, a concentration safely and effectively achievable *in vivo*^{56,57}. Pembrolizumab and balstilimab were used at 50 μ g/mL. For MTT assays, IFN γ and TNF α were used at 1 ng/mL and 10 ng/mL respectively, added to wells at the same time as rabsertib, and incubated for 96 h.

Endogenous ubiquitination assays

The detection of ubiquitinated protein was conducted as previously described³². Briefly, 6×10^6 cells as indicated were treated with MG132 (2 μ M) for 12 h. For T24 experiments, gemcitabine (10 nM) or vehicle (water) was added at the same time as MG132. Cells were lysed in denaturing buffer (50 mM Tris-HCl, 0.5 mM EDTA and 1% SDS) followed by heating at 95° C for 10 min and quenched with nine volumes of quenching buffer (0.5% Triton X-100, 20 mM Tris-HCl (pH 8.0), 137 mM NaCl, 10% glycerol, 2 mM EDTA). Protease inhibitor cocktail was freshly added to all buffers. Cell lysates were incubated on a rotator for 30 min at 4° C then centrifuged at 20,000 \times gravity for 15 min at 4° C. Supernatants were subsequently processed using Dynabeads Protein G for Immunoprecipitation (Thermo Fisher) plus anti-Chk2 antibody (Santa Cruz-5278). The final eluate was processed and immunoblot analysis was performed as described above.

Immunofluorescence, confocal microscopy, and image visualization and analysis

For confocal imaging of PDL1^{mem} and PDL1^{cyto} constructs, cells were grown on collagen-treated slides to

confluence, fixed with 4% fresh formaldehyde/PBS, permeabilized with ice-cold 100% methanol, and blocked in 5% normal goat serum/buffer for 1 h at RT. Cells were incubated with PDL1 primary antibody at 1:1000 overnight at 4° C on a rocker. AlexaFluor secondary antibodies were used at 1:500 for 1 h at RT in the dark, followed by DAPI as nuclear counterstain at 0.1 mg/ml for 5 min. Prolong[®] Anti-Fade mounting agent with #1.5 coverslips was used to seal slides and allowed to dry overnight prior to imaging. Images were taken on Zeiss LSM710 Confocal Microscope using EC Plan-Neofluor 40x/1.30 Oil DIC objective, using same settings between fields of view and cell lines. 16-bit images have dimensions of 1024(x) by 1024(y) and z-dimensions that varied per sample (10–20 z-planes per image).

Cryopreserved ER and PR human ovarian section slides were thawed for 30 min at RT, fixed for 20 min in 4% paraformaldehyde, and washed three times in 1 \times PBS. Samples were permeabilized with 0.1% Triton X-100 for 5 min and blocked in Background Sniper (Biocare Medical, cat #BS966) for 15 min at RT. Antibodies against PDL1 (Abcam #ab205921 or R&D #MAB1561), γ H2AX (Millipore #05–636), and Chk2 (Abcam #ab109413) were diluted with Da Vinci Green (Biocare Medical #PD900L) antibody diluent and incubated overnight at 4° C. After three washes, appropriate fluorophore-conjugated secondary antibodies (AlexaFluor488 or AlexaFluor568, Invitrogen) diluted in Fluorescence Antibody Diluent (Biocare Medical #FAD901L) were incubated for one hour at room temperature. Samples were washed and stained with DAPI (Invitrogen #D1306) and HCS CellMask Deep Red stain (Invitrogen #H32721) for 10 min then mounted in Prolong Gold Anti-fade Mountant (Invitrogen, cat #9071). Stained tissue was imaged by laser scanning confocal microscopy using a Zeiss LSM880 and 20X (0.8 N.A.) Plan/Apo objective with a pinhole aperture of 1–1.5 AU. Images were captured and processed using identical microscope settings (*e.g.*, laser transmission and gain). Quantifications of marker expression from representative 2X zoom images (minimum n=3 patients) were performed using Imaris (Bitplane, v9.0) image analysis software Cells module. The segmentation algorithm detected nuclei via the DAPI channel and the cell body via the far-red channel for CellMask Deep Red, with cell splitting based on one nucleus per cell and cell body signal intensity thresholding using Imaris Image Visualization and Analysis Software 9.9. Statistical analysis was performed by a paired, two-tailed student's t-test with unequal variance. Indirect immunofluorescence of nuclei for Chk2/PDL1 colocalisation was performed as described [57]. Chk2 foci imaging was obtained from pre-extracted nuclei and represent the chromatin-bound fraction. Cells were seeded and grown on glass coverslips for

24 h and if specified, treated with either Chk1i (10 nM) for 12 h or MG132 (5 μ M) for 2 h. Cells were left intact or cell nuclei were pre-extracted as specified for each experiment with nuclear extraction buffer (NEB; 10 mM PIPES (pH 6.8), 100 mM NaCl, 300 mM sucrose, 3 mM MgCl₂, 1 mM EGTA (pH 8.0), 0.5% Triton X-100) for 2 min at room temperature then fixed with 4% paraformaldehyde for 10 min at 4 °C. Nuclei were blocked in 5% BSA and 0.3% Triton X-100 in PBS, immunoblotted with a primary antibody (1:500 in dilution buffer; 1% BSA and 0.3% Triton X-100 in PBS), followed by secondary antibody (2 μ g/mL in dilution buffer). DNA was counterstained with DAPI. Slides were viewed on an Olympus FV3000 confocal microscope. Primary antibodies include rabbit α Chk2 (Abcam), mouse α PDL1 or mouse α GFP (Sigma). Secondary antibodies include α -mouse (Abcam ab150103, Alexa Fluor 647), α -rabbit (Abcam ab150081, Alexa Fluor 488), α -mouse (Abcam ab150117, Alexa Fluor 488), and α -rabbit (Santa Cruz sc362292, CFL-647). Nuclear foci quantification was performed using CellProfiler.

Flow cytometry

Flow cytometry to detect expression of surface proteins in cultured cells was performed as we previously described [10, 11]. For cell death analysis with Annexin V, cells were treated with 1 μ M Chk1 inhibitor (rabusertib) for 48 h. Cells were stained using the Dead Cell Apoptosis Kit with Annexin V for flow cytometry (ThermoFisher V13242) according to the manufacturer protocol. For sorting on PDL1 expression, CTRL T24 cells were stained with α PDL1 antibody (BioLegend 374,508) and sorted on the BD FACS Aria II. For immune analyses, mice were sacrificed using cervical dislocation under isoflurane anesthesia. tumours were collected and strained through 40 micron cell strainers into RPMI-1640 medium. 5×10^6 cells were collected from single-cell suspensions (counted with Vi-Cell-XR cell counter, Beckman Coulter), resuspended in 200 μ L of 1 \times PBS, and transferred to U-bottom 96 well plates. Cells were stained with Live/Dead Cell Stain for UV excitation (ThermoFisher Scientific) for 30 min 4 °C protected from light, followed by incubation with anti-CD16/32 (Biolegend) for 30 min at 4 °C protected from light. Surface antibodies were used at 1:100 and include α CD45 (58–0451-82) from Invitrogen, CD3 (TONBO 80–0032-U100), α CD4 (BD Biosciences 612,952), α CD8 (BD Biosciences 563,786), PD1 (BD Biosciences 566,515), α CD11b (BioLegend 101,226), α CD11c (TONBO 60–0114-U100), α F4/80 (Biolegend 123,135), α Gr1 (BioLegend 108,440), NK1.1 (TONBO 20–5941-U100), and α B220 (BD Biosciences 612,972). After surface staining, cells were washed with FACS buffer (1 \times PBS with 2% FBS), then activated with the Cell Activator Cocktail (Biolegend in

CR10 medium (RPMI-1640 with 10%FBS, L-glutamine, sodium pyruvate, non-essential amino acids, penicillin/streptomycin, HEPES). After 6 h at 37 °C, cells were and permeabilized using the Foxp3/Transcription Factor Staining Buffer Kit (TONBO Biosciences). Following permeabilization, cells were incubated with intracellular antibodies diluted to 1:100 for 30 min at 4 °C. Intracellular antibodies include α FoxP3 (ThermoFisher 15–5773-82), α IFN γ (BD Biosciences 612,769), and α Granzyme B (BioLegend 515,408). After intracellular antibody incubation, cells were washed and fixed. Data were acquired using a Cytex Aurora flow cytometer and analyzed with FloJo software V.10.7.1. For sorting of cultured cells, ES2 cells were stained with Ghost UV 450 (Tonbo 13–0868-T100) Live/Dead stain for 30 min at 4 °C, washed with FACS buffer, then stained for 30 min at 4 °C with isotype control or α PDL1 (Fisher 50–112-8926) then were sorted into PDL1^{lo} or PDL1^{hi} populations using a BD FACSaria Fusion cell sorter.

Small cell lung cancer data sets

44 human SCLC cell lines of the ASCL1 subtype (SCLC-A) [28] were classified based on their PDL1 expression into high and low high groups by a median-centered analysis. IC₅₀ values of DDR inhibitors in the SCLC-A cell lines were determined using a 96-h cell viability assay and calculated as previously described [58] and compared between the PDL1 high and low groups by *t*-test. Grubbs test was used to identify potential outliers.

Protein co-purifications

MBP-PDL1-FLAG (hereby PDL1) and MBP-Chk2-Strep (hereby Chk2) were synthesized and cloned into Series-438A vectors for expression in insect cells [59]. These vectors were transformed into the *E. coli* strain DH10Bac for bacmid generation. Bacmids were PCR verified and transfected into Sf9 (Gibco) insect cells using Cellfectin II Reagent (Gibco) following the manufacturer's instructions for production and amplification of recombinant baculovirus. For co-expression of PDL1 and Chk2, 1 mL of each virus stock was used to infect 50 mL of Tni (Expression Systems) insect cells for 48 h at 27 °C with 150 rpm shaking. Cells were harvested by centrifugation at 1000 \times gravity for 10 min and stored at -80 °C.

We modified a method to test protein complex formation previously described [59]. Briefly, cell pellets were lysed in 20 mL buffer A (25 mM Tris-HCl pH 7.5, 10% glycerol, 0.5 mM EDTA, 200 mM KCl, 1 mM DTT, and 0.01% Igepal CA-630) supplemented with a 4 \times protease inhibitor mix (aprotinin, chymostatin, leupeptin, and pepstatin A at 3 μ g/mL each), 2 μ L benzonase, and 1 mM MgCl₂. Lysates were further processed with 10 strokes in a Dounce homogenizer and sonication at 30% amplitude

using a pulse (10 s on, 30 s off). Clarification of the lysates was accomplished by centrifugation at 45,000 rpm for 45 min in a Type 70 Ti fixed-angle rotor (Beckman Coulter) at 4° C. The supernatant was incubated with 1 mL Anti-FLAG M2 affinity gel (Sigma) for 1 h at 4° C with gentle agitation. The immobilized complex was washed with 50 mL of buffer A before elution in buffer A supplemented with 0.4 µg/mL 1×FLAG peptide across 4 fractions of 1 column volume each. The presence of PDL1 and Chk2 was verified by SDS-PAGE and Coomassie staining, and the elution fractions were pooled before incubation with 500 µL Strep-Tactin Sepharose (IBA) for 1 h at 4° C with gentle agitation. The beads were washed with 50 mL buffer A and eluted in buffer A supplemented with 2.5 mM desthiobiotin in 4 fractions (1 complete volume each). Lysate, flow-through, input, and elutions were run on SDS-PAGE gels, stained with Coomassie blue, and imaged on a ChemiDoc MP Imaging System (Bio-Rad).

Mice, in vivo tumour challenges, and in vivo treatments

Wild type (WT) C57BL/6 J (Bl6), Rag2^{KO} on Bl6 background, and NOD.CgPrkdcscidIl2rgtm1Wj1/SzJ [non-obese diabetic/severe combined immunodeficiency (NOD/SCID)/interleukin (IL)-2Rγ KO, NSG] mice were purchased from Jackson Laboratory or bred in our in-house facility and maintained under specific pathogen free conditions. Mice were given food and water ad libitum. 8 to 10-week old age- and sex matched mice were used. All animals were approved by the UT Health San Antonio Institutional Animal Care and Use Committee or the Dartmouth College Institutional Animal Care and Use Committee. For in vivo 4T1 experiments in NSG mice, CTRL or PDL1^{lo} 4T1 cells (0.5×10^6 cells) were injected into mammary fat pads of BALB-C or NSG mice with Matrigel Membrane Matrix (1:1, Corning). Mice were randomized, and rabusertib in 5% DMSO was administered intraperitoneally 3 times total over the course of the experiment, on day 3 (10 mg/kg) 10 and 17 (1 mg/kg). For in vivo B16 experiments, CTRL or PDL1^{KO} B16 cells (0.5×10^6) were injected into WT mice subcutaneously. 0.2×10^6 CTRL or PDL1^{KO} B16 cells were injected into NSG mice, and 0.4×10^6 PDL1^{KO} B16 cells per flank were injected subcutaneously into Rag2^{KO} mice. Mice were treated with 25 mg/kg rabusertib or vehicle intraperitoneally on day 3, followed by daily injections of 5 mg/kg rabusertib or vehicle. Tumour volumes were measured using Vernier calipers calculated as $(\text{length} \times \text{width}^2)/2$. For in vivo *Nras* mutant melanoma experiments, *CD274^{fl/fl} TN^{61R}* and PDL1 replete *CD274^{+/+} TN^{61R}* (PDL1⁻ NFH1 and PDL1⁺ NCH1, respectively) melanoma cells were challenged into WT Bl6 mice (0.5×10^6 , subcutaneously) and treated with 25 mg/kg rabusertib intraperitoneally starting day 3 and every four

days following, with 5 mg/kg rabusertib every other day. NSG mice received 0.2×10^6 NCH1 or NFH1 cells per flank subcutaneously. Ceftazidime was given 80 mg/kg intraperitoneally daily.

Melanocyte-specific PDL1 knockout genetically engineered mouse melanoma model

In our murine autochthonous melanoma model, mice lack PDL1 only in melanocytes, the melanoma cell-of-origin, and can develop melanomas de novo when induced. To generate these mice, a transgenic mouse with *CD274* flanked by LoxP sites (*CD274^{LoxP}*) on the 129 background from Taconic was crossed onto a BL6 background and then subsequently crossed for 7 generations with a well-established Tyrosinase:Cre^{ERT2} inducible *Nras^{Q61R}* (*TN^{61R}*) mouse melanoma model²⁹. These melanocyte PDL1-deficient mice (*CD274^{fl/fl} TN^{61R}*) or PDL1 replete littermate controls (*CD274^{+/+} TN^{61R}*) were induced by painting 4-hydroxytamoxifen (25 mg/mL in DMSO) on their skin on postnatal day 3 and 4. Mice were induced with 4-hydroxytamoxifen ± ultraviolet B (UVB) radiation on postnatal day 5 using a 312nm 2X8 Watt UVB lamp (Spectroline). We obtained tumour cells from autochthonous melanomas after 4-hydroxytamoxifen induction plus 4.5 kJ/m² UVB radiation and cultured them to create stable cell lines.

RNA-seq and bioinformatics analysis

Total RNA from CTRL, PDL1^{KO}, PDL1^{mem}, and PDL1^{cyto} B16 cells were purified using an RNeasy kit (Qiagen), and RNA quality was ensured on an Agilent Bioanalyzer. 50-base pair single read sequencing was conducted using Illumina HiSeq 2000 at the UT Health San Antonio Genome Sequencing Core Facility. The entire differential expression (DE) analysis and gene set enrichment analysis (GSEA) were performed on R Studio. R package DESeq2 [60] was used to compare differential gene expression analysis. Converting gene IDs to Ensembl IDs was performed with AnnotationDbi. MSigDB was used to obtain the *Mus musculus* gene set. Significant genes were selected by removing those that have a log2FC value of $-2 < x < 2$ post-DE analysis. The fgsea R package was used for enrichment, and ggplot2 was used to visualize GSEA data. Leading edge genes from each pathway (most significant genes driving pathway enrichment) were converted from Ensembl ID to gene symbols using the following website: <https://www.syngoport.org/convert>. Selected genes differentially expressed in PDL1^{KO}/CTRL cells were plotted using R package EnhancedVolcano.

Statistics

Statistical analyses were done using GraphPad Prism 9 software. Data were shown as either mean \pm standard deviation or \pm standard error of the mean where indicated. Unpaired *t*-test was used to determine significance when comparing measurement data from two individual groups. Analysis of variance was used to determine significance when comparing continuous outcomes across multiple experimental groups. Outliers in data sets were identified by Grubb's test and removed from analysis. $P < 0.05$ adjusted for multiple comparisons was considered statistically significant.

Abbreviations

α PD1	Anti-PD1
α PDL1	Anti-PDL1
ATM	Ataxia-telangiectasia mutated
ATR	Ataxia-telangiectasia and Rad3-related protein
Chk1	Checkpoint kinase-1
Chk1i	Chk1 inhibitor
Chk2	Checkpoint kinase-2
CHX	Cyclohexamide
CRISPR	Clustered regularly interspaced short palindromic repeats
CTRL	Control
DAPI	4,6-Diamidino-2-phenylindole
DDR	DNA damage response
DDRi	DNA damage response inhibitor
GSEA	Gene set enrichment analysis
Hi	High
IFN γ	Interferon gamma
KI	Knock-in
KO	Knockout
Lo	Low
RE	Re-expression
PDL1	Programmed death ligand-1
PD1	Programmed death-1
Seq	Sequencing
TNF α	Tumour necrosis factor alpha
γ H2AX	Gamma-H2A histone family member X (S139)

Supplementary Information

The online version contains supplementary material available at <https://doi.org/10.1186/s12943-024-02147-z>.

Supplementary Material 1.
Supplementary Material 2.

Acknowledgements

We thank Agenus for balstilimab. We thank the biostatistics team (Qi Wang and Li Shen) at UT MD Anderson for executing analyses of data sets. We thank Dr. Heather Graham for technical assistance.

Authors' Contributions

C.E.M., A.V.K., and T.J.C. conceived of the ideas, designed experiments, interpreted results, and wrote the manuscript. C.E.M. and A.V.K. performed the experiments with assistance from C.O.O., Y.L., B.P.A., C.R., Z.L., Y.D., S.K., H.B., J.T.B., R.R., C.A.C., M.W., A.S.P., J.M.-L., and H.B.G., for in vitro studies and C.O.O., H.B., H.B.G., Y.D., R.M.R., and A.S.P. for in vivo studies. C.R., B.P.A., and E.V.D. performed biochemistry and imaging. K.R. performed bioinformatic analysis. P.S., W.Z., C.E.B., E.V.D., R.K.V., R.S.S., R.L., Y.H., J.C.G., L.A.B., H.B.G., and Y.D. gave scientific input and helped revise the manuscript. A.S. provided clinical samples and analysis advice. T.J.C. secured funding sources, provided supervision, and performed overall project management and coordination.

Funding

C.E.M. was supported by the Graduate Research in Immunology Program training grant NIH T32 AI138944 and the National Center for Advancing Translational Sciences, National Institutes of Health, through Grant TL1 TR002647. A.V.K. was supported by NCI F30 CA239390. C.O.O. was supported by NCI F31 CA281345. C.E.M., A.V.K., C.O.O., C.A.C., and R.M.R. were supported by the South Texas Medical Scientist Training Program at UT Health San Antonio (T32GM113896). L.B. was supported by NCI CA256780, CA207295, CA070907. E.D. is supported by NIEHS ES035997. R.V. was supported by CA262757. W.Z. was supported by GM141091 and CA268641. E.D. was supported by NIEHS ES035997. P.S. is supported by the NCI (R35 CA241801). T.J.C. received funding from NCI (CA054174, CA268641, CA023108, CA292467), The Clayton Foundation, The Skinner Endowment, the Owens Foundation, Guyre funds, and the Gmelich Chair. R. L. and Y.H. received support from CA279566. The Flow Cytometry Shared Resource at UT Health San Antonio is supported by the NCI (CA054174), the Cancer Prevention and Research Institute of Texas (RP210126), NIH (S10OD030432), and the Office of the Vice President for Research at UT Health San Antonio. The Immune Monitoring and Flow Cytometry Shared Resource at Dartmouth (DartLab) is supported by NCI Cancer Center support grant 5P30 CA023108-41.

Data availability

All data generated and analysed during this study are included in this paper and its supplementary files. Source data are provided with this paper.

Declarations

Ethics approval and consent to participate

Not applicable.

Consent for publication

Not applicable.

Competing interests

TJC and AVK have filed a patent on using PDL1 depleting drugs to treat cancer.

Author details

¹ Graduate School of Biomedical Sciences and Long School of Medicine, University of Texas Health San Antonio, San Antonio, TX, USA. ² Dartmouth Cancer Center and Dartmouth Health, Department of Microbiology and Immunology, Geisel School of Medicine at Dartmouth, Hanover, NH, USA. ³ Department of Biochemistry and Structural Biology, University of Texas Health San Antonio, San Antonio, TX, USA. ⁴ Department of Medicine, University of Texas Health San Antonio, San Antonio, TX, USA. ⁵ Department of Urology, University of Texas Health San Antonio, San Antonio, TX, USA. ⁶ UT Health Mays Cancer Center, University of Texas Health San Antonio, San Antonio, TX, USA. ⁷ Department of Molecular Medicine, University of Texas Health San Antonio, San Antonio, TX, USA. ⁸ UT Southwestern, Dallas, TX, USA. ⁹ Duke Cancer Center, Department of Integrative Immunobiology, Durham, NC, USA. ¹⁰ Department of Thoracic/Head & Neck Medical Oncology, University of Texas MD Anderson Cancer Center, Houston, TX, USA. ¹¹ Department of Gynecologic Oncology & Reproductive Medicine, UT MD Anderson Cancer Center, Houston, TX, USA. ¹² Women's Malignancies Branch, Center for Cancer Research, National Cancer Institute, Bethesda, MD, USA. ¹³ Departments of Molecular Genetics, Cancer Biology and Genetics, The Ohio State University, Columbus, OH, USA. ¹⁴ Dartmouth Health and Dartmouth Cancer Center, Lebanon, NH, USA. ¹⁵ The Geisel School of Medicine at Dartmouth, Hanover, NH, USA. ¹⁶ Department of Immunology, Dartmouth College, Hanover, NH, USA. ¹⁷ Present address: Department of Internal Medicine, New York University Grossman School of Medicine, New York, NY, USA. ¹⁸ Present address: Department of Radiation Oncology, School of Medicine, University of Alabama Birmingham, Birmingham, USA. ¹⁹ Present address: Department of Biochemistry & Molecular Medicine, School of Medicine & Health Sciences, The George Washington University, Washington, DC, USA. ²⁰ Present address: Department of Anatomy & Cell Biology, School of Medicine & Health Sciences, The George Washington University, Washington, DC, USA. ²¹ Department of Integrative Immunobiology, Duke University, Durham, NC, USA.

Received: 7 February 2024 Accepted: 5 October 2024

Published online: 30 October 2024

References

- Topalian SL, Taube JM, Anders RA, Pardoll DM. Mechanism-driven biomarkers to guide immune checkpoint blockade in cancer therapy. *Nat Rev Cancer*. 2016;16:275–87. <https://doi.org/10.1038/nrc.2016.36>.
- Taube JM, et al. Colocalisation of inflammatory response with B7–h1 expression in human melanocytic lesions supports an adaptive resistance mechanism of immune escape. *Sci Transl Med*. 2012;4:127ra137. <https://doi.org/10.1126/scitranslmed.3003689> <https://doi.org/4/127/127ra37>.
- Topalian, S. L., Drake, C. G. & Pardoll, D. M. J. C. o. i. i. Targeting the PD-1/B7-H1 (PD-L1) pathway to activate anti-tumour immunity. 24, 207–212 (2012).
- Paterson AM, et al. The programmed death-1 ligand 1:b7–1 pathway restrains diabetogenic effector T cells in vivo. *J Immunol*. 2011;187:1097–105. <https://doi.org/10.4049/jimmunol.1003496> <https://doi.org/jimmunol.1003496>.
- Dong H, et al. tumour-associated B7–H1 promotes T-cell apoptosis: A potential mechanism of immune evasion. *Nat Med*. 2002;8:793–800.
- Brahmer JR, et al. Safety and activity of anti-PD-L1 antibody in patients with advanced cancer. *N Engl J Med*. 2012;366:2455–65. <https://doi.org/10.1056/NEJMoa1200694>.
- Zou W, Wolchok JD, Chen L. PD-L1 (B7–H1) and PD-1 pathway blockade for cancer therapy: Mechanisms, response biomarkers, and combinations. *Sci Transl Med*. 2016;8:328rv324. <https://doi.org/10.1126/scitranslmed.aad7118>.
- Sharma P, Hu-Lieskovan S, Wargo JA, Ribas A. Primary, Adaptive, and Acquired Resistance to Cancer Immunotherapy. *Cell*. 2017;168:707–23. <https://doi.org/10.1016/j.cell.2017.01.017>.
- Kornepati AVR, Vadlamudi RK, Curiel TJ. Programmed death ligand 1 signals in cancer cells. *Nat Rev Cancer*. 2022;22:174–89. <https://doi.org/10.1038/s41568-021-00431-4>.
- Clark CA, et al. tumour-Intrinsic PD-L1 Signals Regulate Cell Growth, Pathogenesis, and Autophagy in Ovarian Cancer and Melanoma. *Cancer Res*. 2016;76:6964–74. <https://doi.org/10.1158/0008-5472.CAN-16-0258>.
- Gupta HB, et al. tumour cell-intrinsic PD-L1 promotes tumour-initiating cell generation and functions in melanoma and ovarian cancer. *Signal Transduct Target Ther*. 2016;1:1–9. <https://doi.org/10.1038/sigtrans.2016.30>.
- Zhu H, et al. BET Bromodomain Inhibition Promotes Anti-tumour Immunity by Suppressing PD-L1 Expression. *Cell reports*. 2016;16:2829–37. <https://doi.org/10.1016/j.celrep.2016.08.032>.
- Wu B, et al. Adipose PD-L1 Modulates PD-1/PD-L1 Checkpoint Blockade Immunotherapy Efficacy in Breast Cancer. *Oncoimmunology*. 2018;7:e1500107. <https://doi.org/10.1080/2162402X.2018.1500107>.
- Liang J, et al. Verteporfin Inhibits PD-L1 through Autophagy and the STAT1-IRF1-TRIM28 Signaling Axis. Exerting Antitumour Efficacy Cancer immunology research. 2020;8:952–65. <https://doi.org/10.1158/2326-6066.CIR-19-0159>.
- Murray, C. et al. Pharmacologic tumour PDL1 Depletion with Cefepime or Ceftazidime Promotes DNA Damage and Sensitivity to DNA-Damaging Agents. *Int J Mol Sci* 23 (2022). <https://doi.org/10.3390/ijms23095129>
- Kornepati AVR, et al. tumour-intrinsic PD-L1 promotes DNA repair in distinct cancers and suppresses PARP inhibitor-induced synthetic lethality. *Cancer Res*. 2022;82:2156–70. <https://doi.org/10.1158/0008-5472.CAN-21-2076>.
- Tu X, et al. PD-L1 (B7–H1) Competes with the RNA Exosome to Regulate the DNA Damage Response and Can Be Targeted to Sensitize to Radiation or Chemotherapy. *Mol Cell*. 2019;74:1215–26. <https://doi.org/10.1016/j.molcel.2019.04.005>. e1214.
- Marechal, A. & Zou, L. DNA damage sensing by the ATM and ATR kinases. *Cold Spring Harbor perspectives in biology* 5 (2013). <https://doi.org/10.1101/cshperspect.a012716>
- Cleary JM, Aguirre AJ, Shapiro GI, D'Andrea AD. Biomarker-Guided Development of DNA Repair Inhibitors. *Mol Cell*. 2020;78:1070–85. <https://doi.org/10.1016/j.molcel.2020.04.035>.
- Smith, J., Tho, L. M., Xu, N. & Gillespie, D. A. The ATM-Chk2 and ATR-Chk1 pathways in DNA damage signaling and cancer. *Adv Cancer Res* 108, 73–112 (2010). <https://doi.org/10.1016/B978-0-12-380888-2.00003-0>
- Gudmundsdottir, K. & Ashworth, A. The roles of BRCA1 and BRCA2 and associated proteins in the maintenance of genomic stability. *Oncogene* 25, 5864–5874 (2006). <https://doi.org/10.1038/sj.onc.1209874>
- Zhang, D. et al. Bladder cancer cell-intrinsic PD-L1 signals promote mTOR and autophagy activation that can be inhibited to improve cytotoxic chemotherapy. *Cancer medicine* 10, 2137–2152 (2021). <https://doi.org/https://doi.org/10.1002/cam4.3739>
- Rodier, F. et al. Persistent DNA damage signaling triggers senescence-associated inflammatory cytokine secretion. *Nat Cell Biol* 11, 973–979 (2009). <https://doi.org/10.1038/ncb1909>
- Xu G, et al. REV7 counteracts DNA double-strand break resection and affects PARP inhibition. *Nature*. 2015;521:541–4. <https://doi.org/10.1038/nature14328>.
- duplicate with ref 22
- Bartek J, Lukas J. Chk1 and Chk2 kinases in checkpoint control and cancer. *Cancer Cell*. 2003;3:421–9.
- Zaugg, K. et al. Cross-talk between Chk1 and Chk2 in double-mutant thymocytes. 104, 3805–3810 (2007).
- Gay CM, et al. Patterns of transcription factor programs and immune pathway activation define four major subtypes of SCLC with distinct therapeutic vulnerabilities. *Cancer cell*. 2021;39:346–60. <https://doi.org/10.1016/j.ccell.2020.12.014>. e347.
- Hennessey RC, et al. Ultraviolet radiation accelerates NRas-mutant melanomagenesis: A cooperative effect blocked by sunscreen. *Pigment Cell Melanoma Res*. 2017;30:477–87. <https://doi.org/10.1111/pcmr.12601>.
- Gato-Cañas, M. et al. PDL1 signals through conserved sequence motifs to overcome interferon-mediated cytotoxicity. 20, 1818–1829 (2017).
- Burr ML, et al. CMTM6 maintains the expression of PD-L1 and regulates anti-tumour immunity. *Nature*. 2017;549:101–5. <https://doi.org/10.1038/nature23643>.
- Mezzadra R, et al. Identification of CMTM6 and CMTM4 as PD-L1 protein regulators. *Nature*. 2017;549:106–10. <https://doi.org/10.1038/nature23666>.
- Gao Y, et al. Acetylation-dependent regulation of PD-L1 nuclear translocation dictates the efficacy of anti-PD-1 immunotherapy. *Nat Cell Biol*. 2020;22:1064–75. <https://doi.org/10.1038/s41556-020-0562-4>.
- Hou J, et al. PD-L1-mediated gasdermin C expression switches apoptosis to pyroptosis in cancer cells and facilitates tumour necrosis. *Nat Cell Biol*. 2020;22:1264–75. <https://doi.org/10.1038/s41556-020-0575-z>.
- Zannini L, Delia D, Buscemi G. CHK2 kinase in the DNA damage response and beyond. *Journal of molecular cell biology*. 2014;6:442–57. <https://doi.org/10.1093/jmcb/mju045>.
- Zannini, L., Delia, D. & Buscemi, G. J. J. o. m. c. b. CHK2 kinase in the DNA damage response and beyond. 6, 442–457 (2014).
- Satelli, A. et al. Potential role of nuclear PD-L1 expression in cell-surface vimentin positive circulating tumour cells as a prognostic marker in cancer patients. *Scientific reports* 6, 28910 (2016). <https://doi.org/10.1038/srep28910>
- Wei Y, et al. The local immune landscape determines tumour PD-L1 heterogeneity and sensitivity to therapy. *J Clin Invest*. 2019;129:3347–60. <https://doi.org/10.1172/JCI127726>.
- Bohgaki, M. et al. The E3 ligase PIRH2 polyubiquitylates CHK2 and regulates its turnover. *Cell Death Differ* 20, 812–822 (2013). <https://doi.org/10.1038/cdd.2013.7>
- Labay, E. et al. Repurposing cephalosporin antibiotics as pro-senescent radiosensitizers. *Oncotarget* 7, 33919–33933 (2016). <https://doi.org/10.18632/oncotarget.8984>
- Sen T, et al. Targeting DNA Damage Response Promotes Antitumour Immunity through STING-Mediated T-cell Activation in Small Cell Lung Cancer. *Cancer Discov*. 2019;9:646–61. <https://doi.org/10.1158/2159-8290.CD-18-1020>.
- Farkkila, A. et al. Immunogenomic profiling determines responses to combined PARP and PD-1 inhibition in ovarian cancer. *Nature communications* 11, 1459 (2020). <https://doi.org/10.1038/s41467-020-15315-8>
- Drerup JM, et al. CD122-Selective IL2 Complexes Reduce Immunosuppression, Promote Treg Fragility, and Sensitize tumour Response to PD-L1 Blockade. *Cancer Res*. 2020;80:5063–75. <https://doi.org/10.1158/0008-5472.CAN-20-0002>.
- Pilie PG, Tang C, Mills GB, Yap TA. State-of-the-art strategies for targeting the DNA damage response in cancer. *Nat Rev Clin Oncol*. 2019;16:81–104. <https://doi.org/10.1038/s41571-018-0114-z>.
- dup. of ref. 45
- Li, Q. et al. A new wave of innovations within the DNA damage response. *Signal Transduct Target Ther* 8, 338 (2023). <https://doi.org/10.1038/s41392-023-01548-8>
- Ditano JP, Eastman A. Comparative Activity and Off-Target Effects in Cells of the CHK1 Inhibitors MK-8776, SRA737, and LY2606368. *ACS Pharmacol Transl Sci*. 2021;4:730–43. <https://doi.org/10.1021/acspsci.0c00201>.

48. Toledo LI, et al. A cell-based screen identifies ATR inhibitors with synthetic lethal properties for cancer-associated mutations. *Nat Struct Mol Biol*. 2011;18:721–7. <https://doi.org/10.1038/nsmb.2076>.
49. Buisson R, Boisvert JL, Benes CH, Zou L. Distinct but Concerted Roles of ATR, DNA-PK, and Chk1 in Countering Replication Stress during S Phase. *Mol Cell*. 2015;59:1011–24. <https://doi.org/10.1016/j.molcel.2015.07.029>.
50. Saldivar JC, Cortez D, Cimprich KA. The essential kinase ATR: ensuring faithful duplication of a challenging genome. *Nat Rev Mol Cell Biol*. 2017;18:622–36. <https://doi.org/10.1038/nrm.2017.67>.
51. Kornepati AVR, Rogers CM, Sung P, Curiel TJ. The complementarity of DDR, nucleic acids and anti-tumour immunity. *Nature*. 2023;619:475–86. <https://doi.org/10.1038/s41586-023-06069-6>.
52. Chakravarty D, et al. Extranuclear functions of ER impact invasive migration and metastasis by breast cancer cells. *Cancer Res*. 2010;70:4092–101. <https://doi.org/10.1158/0008-5472.CAN-09-3834>.
53. Hasty P, et al. eRapa Restores a Normal Life Span in a FAP Mouse Model. *Cancer Prev Res (Phila)*. 2014;7:169–78. <https://doi.org/10.1158/1940-6207.CAPR-13-0299>.
54. Clark CA, Gupta HB, Curiel TJ. tumour cell-intrinsic CD274/PD-L1: A novel metabolic balancing act with clinical potential. *Autophagy*. 2017;13:987–8. <https://doi.org/10.1080/15548627.2017.1280223>.
55. Lin, C. et al. Ceftazidime is a potential drug to inhibit SARS-CoV-2 infection in vitro by blocking spike protein-ACE2 interaction. *Signal Transduct Target Ther* 6, 198 (2021). <https://doi.org/10.1038/s41392-021-00619-y>
56. Ramon-Garcia, S. et al. Repurposing clinically approved cephalosporins for tuberculosis therapy. *Scientific reports* 6, 34293 (2016). <https://doi.org/10.1038/srep34293>
57. de la Pena Avalos, B. & Dray, E. Visualization of DNA Repair Proteins Interaction by Immunofluorescence. *Journal of visualized experiments : JoVE* (2020). <https://doi.org/10.3791/61447>
58. Cardnell RJ, et al. Proteomic markers of DNA repair and PI3K pathway activation predict response to the PARP inhibitor BMN 673 in small cell lung cancer. *Clin Cancer Res*. 2013;19:6322–8. <https://doi.org/10.1158/1078-0432.CCR-13-1975>.
59. Gradia SD, et al. MacroBac: New Technologies for Robust and Efficient Large-Scale Production of Recombinant Multiprotein Complexes. *Methods Enzymol*. 2017;592:1–26. <https://doi.org/10.1016/bs.mie.2017.03.008>.
60. Love, M. I., Huber, W. & Anders, S. Moderated estimation of fold change and dispersion for RNA-seq data with DESeq2. *Genome Biol* 15, 550 (2014). <https://doi.org/10.1186/s13059-014-0550-8>

Publisher's Note

Springer Nature remains neutral with regard to jurisdictional claims in published maps and institutional affiliations.